Dissertation

Exploring lipid-mediated TRPC signaling by light

submitted by

Oleksandra Tiapko

for the Academic Degree

of

Doctor of Philosophy

at the

Medical University of Graz

Institute / Gottfried-Schatz-Research-Center – Biophysics

Supervision of

Prof. Dr. Klaus Groschner

2018

Declaration

I hereby declare that this PhD thesis is my own original work and data. I have fully acknowledged by name all of those individuals and organizations that have contributed to the research for this thesis. Due acknowledgement has been made in the text to all other material used. Throughout this thesis and in all related publications I followed the „Standards of Good Scientific Practice and Ombuds Committee at the Medical University of Graz".

Graz, 29.11.2018 Signature

Disclosure

This doctoral thesis contains parts of the two published manuscripts:

1) **Tiapko O[1],** Bacsa B[1], la Cruz de GG[2], Glasnov T[2], Groschner K[1]. Optopharmacological control of TRPC channels by coumarin-caged lipids is associated with a phototoxic membrane effect. Sci China Life Sci. 2016 Jul 19;59(8):802–10.

2) Lichtenegger M[1*], **Tiapko O[1*]**, Svobodova B[1], Stockner T[3], Glasnov T.N[2], Schreibmayer W[1], Platzer D[1], de la Cruz G.G[2], Krenn S[1], Schober R[4], Shrestha N[1], Schindl R[1], Romanin C[4] and Groschner K[1] An optically controlled probe identifies lipid-gating fenestrations within the TRPC3 channel. Nature Chemical Biology. Springer US; 2018 Feb 23;14(4):1–9.

[1]Institute of Biophysics, Medical University of Graz, Graz, Austria; [2]Institute of Chemistry, University of Graz, Graz, Austria; [3]Institute of Pharmacology, Medical University of Vienna, Vienna, Austria; [4]Institute of Biophysics, University of Linz, Linz, Austria. * contributed equally

I hereby confirm, that all co-authors have explicitly agreed to the use of their data in this work.

Acknowledgements

First of all, I would like to express my sincere gratitude to my advisor Prof. Klaus Groschner. Your support and encouragement made my research work so interesting and led me to the spectacular results. I am very thankful for the scientific and especially writing guidance you showed me. And I genuinely value every piece of advice and all the discussions we had for the last four years.

I am very grateful to the DK-MCD PhD program and the Austrian Science Fund (FWF) and the Medical University of Graz for the financial support.

I would also like to thank my committee members Wolfgang Graier, Georg Pabst, Harald Janovjak and Helmut Kubista for advising, suggesting and supporting my scientific work.

Additionally, special gratitude I want to address to Helmut Kubista for teaching me basics of neurophysiology. Your advices and mentoring me during these years are invaluable.

I want to thank my colleagues Bernadett Bacsa, Michaela Lichtenegger, Sarah Krenn, Sanja Curcic, Annarita Graziani and Niroj Shresta. Your help, support and friendship mean everything to me.

I am very happy and thankful for the chance to work with Toma Glasnov and Gema Guedes de la Cruz for the last four years. All the work you put into creating and synthesizing the photoswitches was so stimulating and motivating for me that I had to test them immediately.

I am thankful for the immense help and contribution of my group members. Michaela Janschitz, Patrick Wiedner and Gebhard Schratter, your advice, help and expertise supported my continuous work and gave me an opportunity to achieve a lot.

I thank to my family for all the love and support they gave me. I am so thankful to my beloved parents who raised me and supported my carrier choice. My brother, grandmother and aunts for being there for me all these years. And the most of all my loving, patient and understanding future husband Oliver Mahler. My gratitude for your support in the last years of my PhD is beyond words.

Thank you all sincerely!

Table of Contents

1. Abbreviations and Definitions

- 1,2-DOG/DiC8 – 1,2-dioctanoyl-sn-glycerol
- Bhcmoc-1,2-DOG – 6-bromo-7-hydroxycoumarin-4- ylmethoxycarbonyl phototriggered 1,2-di-*O*-octanoyl glycerol
- BI – 1,3-dihydro-2*H*-benzo[*d*]imidazol-2-one
- Cryo-EM – electron cryomicroscopy
- GFP – green fluorescent protein
- GSK – GSK1702934A
- HEK293 – human embryonic kidney cells
- I-V relation – current to voltage relation
- IP_3 – inositol 1,4,5-trisphosphate
- NMDG – N-Methyl-D-glucamin
- OAG – 1-oleoyl-2-acetyl-sn-glycerol
- OptoGArG – 3-((2-nitrobenzyl)oxy)propane-1,2-diyl-*bis*(4-(4-((*E*)-(4-butylphenyl)diazenyl)phenyl)butanoate
- PhoDAG-1 – [(2S)-2-[4-[4-[(4-butylphenyl)diazenyl]phenyl]butanoyloxy]-3-hydroxypropyl] octadecanoate
- PI – 1,3-dihydro-2*H*-imidazo[4,5-*b*]pyridin-2-one derivative
- PKC – protein kinase C
- PLC – phospholipase C
- Pyr3 – pyrazole 3
- R-GECO – genetically encoded Ca^{2+} sensor
- SAG – 1-stearoyl-2-arachidonoyl-sn-glycerol
- TM – transmembrane helix
- TRPC – transient receptor potential
- UV – ultraviolet
- YFP – yellow fluorescent protein
- PIP_2 – phosphatidylinositol 4,5-biphosphate

2. Abstract in German

Einleitung: TRPC3 Kanäle haben durch ihre Bedeutung in erregbaren und nicht erregbaren Zellen und ihrem einzigartigen Aktivierungsmechanismus, viel Aufmerksamkeit auf sich gezogen. Die Entschlüsselung des Prinzips der Lipiderkennung durch TRPC-Kanäle und die Klärung ihrer exakten Rolle in nativen Zellen erfordert die Entwicklung spezifischer Strategien. Die Photopharmakologie als neuartige und hochpräzise Methode zur Manipulation von Signalmolekülen eröffnet die Möglichkeit zu einer solch spezifischen Kontrolle von TRPC Kanälen. Diese Technik bietet zwei prinzipielle Ansätze die zur optische Kontrolle von TRPC3-Kanälen geeignet sind: “caged” und “photochrome” second messenger. Die Lichtgesteuerte Aktivierung von Liganden kann mechanistische Einblicke in die Signalfunktion von TRPC3 liefern und ihre Nutzung als therapeutische Zielstruktur vorantreiben.

Ziel: Die Entwicklung spezifischer photopharmakologischer Werkzeuge zur Manipulation der TRPC3-Kanalaktivität in vitro und in vivo.

Materialien und Methoden: In dieser Arbeit haben wir photoschaltbare Liganden auf ihre Eignung zur Kontrolle von TRPC3-Kanälen durch Licht untersucht. Wir kombinierten elektrophysiologische Methoden mit Ca^{2+} “Imaging”-Techniken, um die Aktivität von TRPC3 während der Photoaktivierung mittels Lipid- und Nicht-Lipid-Aktivatoren, nachzuweisen. Neben einem Standard Expressionssystem (HEK293) wurden zwei weitere Zellmodelle (Endothelzellen und Neuronen) mit endogen exprimierten TRPC-Kanälen zur Charakterisierung dieser photopharmakologischen Werkzeuge verwendet.

Ergebnisse und Schlussfolgerung: “Lipid-uncaging” bewirkte Ca^{2+} -Transienten in TRPC3-transfizierten Zellen. Allerdings wurde dabei eine “uncaging”-induzierte Leitfähigkeit als ein unerwartetes

UV-beleuchtungsabhängiges Artefakt identifiziert. Dieser Nebeneffekt war durch die Käfigstruktur (Coumarin) erzeugt und berut vermutlich auf einer direkten Wirkung auf die LIpidmembran. Alternativ haben wir zu umgeheung dieser Probleme photochrome Liganden entwicklet. Photochrome Gruppen wie Azobenzol

ermöglichen die Kontrolle des Konformationszustands durch lichtabhängige cis-trans-Isomerisierung und damit der biologischen Aktivität eines Liganden. Der Einbau von Azobenzol in Lipide wurde als eine Alternative zur “uncaging”-Strategie eingesetzt. Ein Mutagenesescreening, das durch Homologie-Modellierung von TRPC3 in Kombination mit photosensitiven Lipiden durchgeführt wurde, ermöglichte die Identifizierung einer essentiellen Lipid-Protein-Interaktionsstelle innerhalb des Porenkomplexes von TRPC3. Um eine noch spezifischere Kontrolle über endogene Kanäle zu erreichen, synthetisierten wir ein photochromes Benzimidazol OptoBI-1, ein Derivat des TRPC3/6-Agonisten (GSK1702934A) Die Lichtstimulation von OptoBI-1 ermöglichte eine präzise Kontrolle über TRPC-Kanäle in Endothelzellen und Neuronen. Zusammenfassend liefert diese Arbeit eine Grundlage für die Entwicklung zukünftiger Strategien zur Erforschung von TRPC-Kanälen *in vitro* und *in vivo*.

3. Abstract in English

Introduction: TRPC3 channels have been attracting much attention through the years with its unique mechanism of activation, which results in Ca^{2+} influx in excitable and non-excitable cells. Deciphering the principle of ligand recognition by TRPC channels and clarifying their exact role in native cells demands specific tools. Photopharmacology as a novel and highly precise technique for manipulation of signaling molecules opens a venue for targeting TRPC3 with high temporal and spacious precision. The technique offers two strategies, which are suitable for optical control of TRPC3 channels: caged and photochromic second messengers. Light-controlled activation of channel activating ligands may provide mechanistic insights into the signaling function of TRPC3 and advance their therapeutic targeting.

Aim: we set out to develop specific photopharmacological tools for manipulation of TRPC3 channel activity and function *in vitro* and *in vivo*.

Materials and methods: In this work we characterized photoswitchable ligands for suitability to control TRPC3 channels by light. We combined electrophysiological and Ca^{2+} imagine techniques to detect activity of TRPC3 overexpressed in HEK293 cells during photoactivation of lipid- and non-lipid activators. Additionally, two cell models (endothelial cells and neurons) with endogenously expressed TRPC channels were used to characterize the selectivity of these photopharmacological tools.

Results and conclusion: Lipid uncaging induced Ca^{2+} transients in TRPC3 transfected cells. However, the uncaging-induced conductance was identified as an unexpected UV illumination-dependent artifact, which was produced by the cage structure. Therefore, caging structures in photopharmacological experiments have to be used with caution. Photochromic moieties like azobenzene allows for control of the conformational state by light dependent cis-trans isomerization and, thereby of the biological activity of a ligand. Azobenzene incorporation into lipids was employed as an alternative to the uncaging strategy. A mutagenesis screen, guided by homology modeling of TRPC3 in combination with utilization of photosensitive lipids revealed an essential lipid-protein interaction site within the pore complex of TRPC3. To exert a more specific control over endogenous channels, we synthetized a photochromic

derivative of the TRPC3/6 agonist GSK1702934A and assigned this benzimidazole derivative as OptoBI-1. Light-stimulation of OptoBI-1 enabled precise control over TRPC channels in endothelial cells and neurons. In summary, this work provides a basis for a development of future strategies to explore TRPC channels *in vitro* and *in vivo.*

4. Introduction to TRPC3

TRPC family exhibits the the closest structural relation to *trp* channels, which were first discovered in the *Drosophila* compound eye. TRPCs are plasma membrane-resident, non-selective cation channels with partial selectivity for Ca^{2+} over other cations. This family is highly expressed all over the body and plays a crucial role in many cellular processes (1-3) (4).

TRPC channel consists of 6 transmembrane helixes (TM1-6) with a pore-forming region localized between TM5 and TM6. Four subunits form a tetramer as a functional channel. The cytosolic part of each of the subunits contains 3-4 ankyrin repeats, a coil-coiled region and a putative caveolin-binding region in the N-terminus. T-terminus has of a TRP-box, a highly conserved prolin-rich motif, a calmodulin/IP_3 receptor binding (CIRB) and coil-coiled regions in the C-terminus (5,6) (4).

TRPCs share ≥30% homology among each other. Based on sequence comparison, TRPCs can be divided into two subgroups: TRPC1/4/5 and TRPC2/3/6/7. *Trpc2* is responsible for pheromone sensing in rodents but represents a pseudogene in humans. Members of the TRPC family are widely expressed within the whole body and play significant role in multiple cellular processes. Homotetramers of TRPC1/4/5 were initially suggested as store-operated channels and just recently demonstrated as lipid-sensitive (7), while TRPC3/6/7 were already early on recognized as lipid-gated channels (5,8). All TRPCs can form functional heterotetramers with distinct activation pattern, current-to-voltage relation and conductance (9) (4).

Transient receptor potential canonical 3 (TRPC3) channels displays a few outstanding features among other TRPCs. It is constitutively active and appears pre-opened to allow a background cation influx into the cells. These pores formed by TRPC3 are slightly more selective to Ca^{2+} over other cations with a permeability ration P_{Ca}/P_{Na} = 1.6 ± 0.27 and a single channel conductance 23 pS (10). TRPC3 channels display a distinct I-V relation with prominent inward current and a reversal potential at around 0 mV (11). Interestingly, TRPC3 channels show remarkable Ca^{2+}-

sensitivity therefore removal of extracellular Ca^{2+} results in elevation of basal activity and ligand-induced response (10) (4).

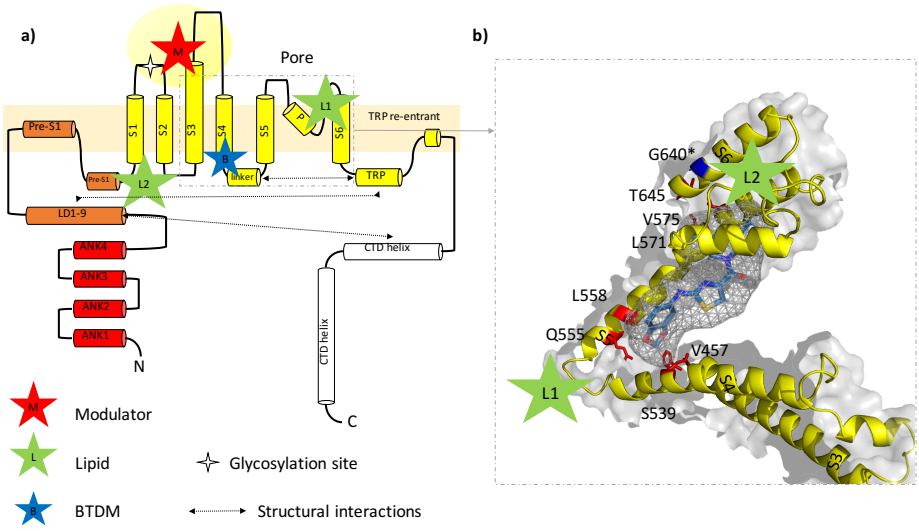

Figure 1. Ligand-channel interactions and potential drug binding sites in TRPC3. (a) Schematic illustration of the domain structure of one TRPC3 channel subunit according to the information provided in from Fan et al. **(12)**. Lipid binding sites (green stars) are indicated with L1 (formed by LD9, pre-S1, S1, S4, and S4–S5 linker) and L2 (between p-loop and S6 helix); potential modulator binding site (M) represented by a cavity (extracellular domain) formed by the extended S3 helix, S1–S2 and S3–S4 linkers as previously identified **(12)**. Proposed BTDM binding site formed by S3, S4–S5 linker, S4, S5, and S6 identified by Tang et al. **(13)**. (b) Detailed view on postulated 2-(benzo[d][1,3]dioxol-5-ylamino)thiazol-4-yl) ((3S,5R)-3,5-dimethylpiperidin-1-yl)methanone (BTDM) binding site in TRPC3: amino acids in the TRPC3 sequence, corresponding to the TRPC6 BTDM binding site are marked in red. The glycine residue G652 (here G640, isoform 1/Q13507-1 in UniProt) identified as crucial for recognition and accommodation of lipid activators is highlighted in blue **(14)**. The BTDM molecule is schematically placed into the proposed binding site ("Reproduced from **(4)** with permission of publisher Cells, 2018" (https:// creativecommons.org/licenses/by/4.0/)).

4.1 Potential role of TRPC3 in human disease

As a protein ubiquitously expressed in the body and involved in maintenance of Ca^{2+} concentration in cytoplasm, TRPC3 activity affects function of excitable and non-excitable cells. For example, TRPC3 expression was detected in the Purkinje cells of cerebellum (15) and in hippocampal neurons (16). Becker et al. found that a gain-of-function mutation (T635A; designated as *Mwk* mutation) in TRPC3, which is

associated with enhanced currents through TRPC3 channels in cerebellum. This leads to degradation of Purkinje cells with consequent impaired coordination control in mice (17). Later, Fogel et al. found a similar mutation in adult-onset spinocerebellar ataxia in human caused by mutation in TRPC3 channels (A762H) resulting in Purkinje cells death (18). Importance of TRPC3 function in hippocampal neurons was shown by Neuner et al. Inhibition of the basal activity of these channels was found to increase neuronal firing, which resulted in better space orientation and improved contextual fear memory in mice (16). However, the signaling of TRPC3 channels in hippocampal neurons was not analyzed in detail (4).

In non-excitable cells such as endothelial cells, TRPC3 channels contribute to a Ca^{2+} influx through the plasma membrane, which was initially considered as store-dependent or store-operated, but later on identified as receptor-operated. TRPC3 induced Ca^{2+} changes in the cytoplasm facilitate the activity of a constitutively expressed, Ca^{2+} regulated nitric oxide synthase NOS III (19) and production of nitric oxide (NO) which leads to vasodilatation (20). Therefore, development of a specific strategy to target TRPC3 channels in this tissue appears attractive in terms of therapeutic interventions (4).

4.2 Endogenous and synthetic channel activators

TRPC3 channels were found overexpressed in many pathophysiological processes but their primary function in cell is not well-defined yet. Many efforts were undertaken to specifically manipulate TRPC3 channels in their natural environment. A distinct feature of TRPC family is the interaction of these channels with plasma membrane lipids like PIP_2 (21) and PLC-produced or synthetic (SAG, OAG, DOG) diacylglycerols (8). Both lipid species were found to promote TRPC activity. Therefore, understanding of the lipid-sensing machinery would advance novel drug development for TRPC3 determined targeting (4).

Importantly, the manipulation of endogenous TRPC3 channels by lipids has certain limitations including the lack of control over time dependent changes in the level of lipid activators at the channel. As an alternative to lipid-mediated control, two synthetic non-lipid activators were introduced: GSK1702934A (GSK) and

pyrazolepyrimidine-based agonists (22,23). Both of these actuators activate lipid-sensitive TRPC channels bypassing PLC pathway. GSK exerts its action *in vitro* and *in vivo* by eliciting TRPC3- and TRPC6-like currents as demonstrated in in TRPC overexpressing HEK293 cells. In addition, GSK (1 μM) transiently increased blood pressure in conscious Sprague Dawley rats (22). Later, Doleschal et al. confirmed the selectivity of GSK by applying it to freshly isolated cardiomyocytes. GSK was unable to induce currents in cardiomyocytes at a low level of endogenous TRPC3 expression, while TRPC3-transfected cardiomyocytes perfused with GSK showed a TRPC3-like conductance. TRPC3 overexpressing cardiomyocytes displayed a prolonged, late repolarization phase during the action potential when perfused with GSK (24). Lately, Qu et al. introduced pyrazolepyrimidine-based agonists which exhibited a high potency (EC50 in the nanamolar range). New small molecule agonists were apparently selective towards ligand-gated TRPC channels and not affecting other TRP family members (23). However, their action *in vivo* was not confirmed yet (4).

TRPC3 has been identified to promote proliferative cell phenotypes (25-27), dendrite growth, nitric oxide production and motor coordination. Both natural and synthetic activators, efficiently promote the activity of overexpressed TRPC3s in cell lines and isolated cells. However, classical ligand application lacks tissue specificity and the spatiotemporal precision to efficiently target TRPC3s in a particular type of cells. Therefore, a nove and unconventional approach that provides high spatial and temporal intervention such as photopharmacology may open the perspective of therapeutic targeting of these ligand-gated TRPCs (4).

4.3 Photopharmacology as a therapeutic perspective

Photopharmacology is a noninvasive and remote way to control biological processes within cells *in vitro* and *in vivo.* It was developing fast in the last decades and already gained importance due to its advantages over traditional ways of govern cell activity. There are two main ways to control drugs by light and without genetic innervation into protein expression. First the photopharmacological approach uses a light-sensitive caging agent to block the activity of the bioactive molecule. The cage is

an inert moiety, which is fused via covalent bond to the molecule. A particular wavelength (usually UV) releases the ligand from the caging moiety to allow interaction with its biological target. The very first attempt to employ photopharmacology in TRPC studies was reported by Nadler et al. The group used caged DAGs to monitor TRPC3/6 activity in HeLa cells (28). Coumarin and nitroveratroyl were used as caging agents to prevent the interaction of DAGs (SAG and DOG) with the channels (28). Short UV light illumination released DAG species leading to Ca^{2+} concentration increase in cytoplasm of HeLa cells. $NiCl_2$ and other non-selective blockers of TRPCs such as SKF-96365 effectively inhibited the response in HeLa cells after DAGs photouncaging, suggesting TRPC-dependent Ca^{2+} influx in these cells (28) (4).

A second photopharmacological approach is to use photochromic ligands for reversible light-induced intervention and manipulation of proteins. Azobenzene as a light-sensing moiety with a *cis-trans* flexible conformation is the most frequently used photopharmacological tool. Azobenzene incorporation into side chains of the DAGs was successfully used to control lipid-dependent proteins. Frank et al. introduced azobenzene fused SAG and two 1,2-DOG photoswitches (PhoDAG-1 and PhoDAG-2 and PhoDAG-3 respectively). PhoDAGs in the *trans*-state caused little or no effect on PKC alpha activation and translocation as demonstrated by overexpression in HeLa cells. In addition, photoswitchable lipids in *trans*-state had no impact on proteins (Munc 13) involved into neurotransmitter release and activity of pancreatic β cells. On the contrary, UV-induced *cis*-isomerization of PhoDAGs was very efficient in triggering lipid-dependent processes in the cells (4).

Leinders-Zufall et al. continued this approach to explore the advantages of photoswitchable DAGs, by using PhoDAG-1 and PhoDAG-3 as tools to study mTrpc2 and hTRPC6 channels. mTrpc2 channels are mostly found in sensory neurons of vomeronasal and main olfactory organ. Photopharmacological control of TRPC2 with exceptionally high spatial precision by PhoDAGs allowed to localize and specify role of mTrpc2 channels in VNO and main olfactory organ. In addition, they showed a

light-dependent control with PhoDAGs over other lipid-sensitive TRPC members, like TRPC6, overexpressed in HEK cells (4).

Considering the advantages of photopharmacology, light-sensitive tools are highly valuable to decipher essential molecular features of TRPC channels and to uncover their specific role in cells and tissues.

5. Aim

The central aim of the project was to develop tools to study TRPC3 channels with high temporal, spatial and quantitative precision. Therefore, we developed three different photopharmacological ligands to explore the lipid recognition of TRPC3 channels and specifically target them in native tissue:

1) Characterizing caged lipids for suitability to study TRPC3 channels

The main advantage of a caged ligand approach is that the released/uncaged biomolecule has a non-modified structure. Photouncaging of diacylglycerols was shown to trigger Ca^{2+} transients in HELa cells, which express TRPC3/6 channels. Therefore, we explored the suitability of coumarin-caged lipids for spatiotemporal control over TRPC3 channels (29).

2) Exploring the lipid-sensing machinery of TRPC3 with photoconvertible lipids

Photochromic ligands allow for a fast and reversible light-dependent control over bioactivity of a molecule in proximity to the protein of interest. We combined photoswitchable DAG (OptoDArG) with structural mutagenesis to study the lipid-protein interaction of TRPC3 channels (14).

3) Targeting of TRPC channels in native tissue with photopharmacological synthetic ligands

Lipid-gated TRPC channels are highly expressed in neuronal- and cardiovascular tissues. Precise pharmacological control over their activity in native cells can provide important insights into organ function/dysfunction. Therefore, we aimed to control endogenously expressed channels in endothelial cells and neurons with a photoderivative of synthetic activator GSK1702934A.

6. Methods

6.1 Cell culture and transfection

Human embryonic kidney 293 (HEK293) and human umbilical vein endothelium derived (EA.hy926) cells were cultured in Dulbeco's Modified Eagle Medium (DMEM, Invitrogen,) with 10%supplemente of fetal bovine serum (FBS), streptomycin (100 µg/mL), penicillin (100 U/mL), L-glutamine (2 mM/L) and HEPES (10 mM/L) in constant at 37°C and 5% CO_2 level.

HEK293 cells were seeded in 3,5 cm dishes and EA cells were seeded in flask the day before the transfection and when reached approximately 80% confluency grown were transiently transfected with 5 µg plasmid DNA using Lipofectamine2000 (Lifetechnologies) according to the manufacturer's protocol. Cells were reseeded on 6x6 mm glass cover slips 24 h after transfection.

6.2 Mice handling

Mixed strain background mice (Balb/c – C57/Bl6; WT) were used for experiments of cultured hippocampal neurons. A TRPC1-7 (hepta) KO (Balb/c – C57/Bl6) mouse model was generated as described (30) and used as a control.

6.3 Dissociated hippocampal neurons

Both WT and KO mice (P0) were used for preparation of dissociated hippocampal neurons. Newborn mice were killed immediately after birth by decapitation in full accordance with all rules of the Austrian animal protection law and the Austrian animal experiment by-laws.

Hippocampi were isolated from the hemispheres in cold buffer containing (in mM): 137 NaCl, 4.5 KCl, 1.1 Na_2HPO_4 × 2 H_2O, 1.1 KH_2PO_4, 6.1 glucose, and 1 kynurenate, pH adjusted to 7.3 with NaOH. For chemical dissociation 20 min of incubation with papain at 37°C following by mechanical dissociation. Neurons were seeded into 3,5 cm dishes with antibiotic-containing DMEM high glucose with 2 mM L-glutamine supplemented with 10% heat-inactivated inactivated fetal bovine serum (Biochrom) and 12.5 mg/ml ITSS (Insulin-Transferrin-Sodium Selenite Supplement,

Roche), 10 nM progesterone (Sigma Aldrich) and antibiotics (25,000 IU/l penicillin and 25 mg/l streptomycin, Sigma Aldrich). After 24h the medium was changed to antibiotic-free and neurons were kept at 37°C and 5% CO_2 level for 12-14 days before the experiments.

6.4 mRNA isolation and qPCR

Total RNA was isolated using PEQLAB total RNA isolation kit (Peqlab) and reverse transcription was performed in a thermal cycler (Peqlab) using a high-capacity cDNA reverse transcription kit (Applied Biosystems). TRPC3 knock-down efficiency was determined by quantitative RT-PCR using the GoTaq® qPCR master mix (Promega). RT-PCR was performed on a LightCycler 480 (Roche Diagnostics). Relative expression of the target gene was normalized to human GAPDH, as a reference gene. Primers for real-time PCR were purchased from Eurofins Genomics (Ebersberg, Germany) and had the following sequences: hTRPC3 for: 5'-ACGACTTCTACGCTTACGACGAG -3', hTRPC3 rev: 5'-CTTAATGGCAAGTTTGACACGAC-3'.

6.5 Ca^{2+} imaging

For Ca^{2+} imaging, HEK293 cells were co-transfected YFP-TRPC3 and red-shifted genetically encoded Ca^{2+} sensor R-GECO or R-GECO only (R-GECO1.2, kindly provided by Dr. R. Mally) and seeded on cover slips the day prior to the experiments. For detection of Ca^{2+} changes in cytoplasm during the experiments, cells were illuminated with 570 nm. Cells during the experiment were kept in Tyrode buffer containing (mM): 140 NaCl, 5 KCl, 2 $CaCl_2$,1 $MgCl_2$, 10 HEPES and 10 glucose, pH 7.4 adjusted with NaOH). For control experiments, cells were exposed to DMSO instead of the light-sensitive activators.

Non-transfected or transfected with CFP-TRPC3 EA.hy 926 were seeded on glass cover slips the day before the experiments. For Ca^{2+} imagine, cells were preincubated for 20 min at room temperature in dark in Ca^{2+} sensitive dye Fluo-4 AM (ThermoFisher Scientific). After incubation, the cover slip was transferred to a cell bath on an inverted microscope with 40×1.3 N.A. oil-immersion objective (Olympus

IX71) with Tyrode buffer at room temperature. Cells were excited at 490 nm every second and UV light for photoconversion was applied two times for 15 sec between the Flou-4 AM excitation. Fluo-4 fluorescence bleaching was corrected by calculating the bleaching function Fb for each individual cell using a one phase exponential decay equation for curve fitting and $[Ca^{2+}]_i$ is represented as F/Fb.

An Oligochrome light source (Till Photonics) was used and fluorescent images were captured every second with an ORCA-03G digital CCD camera (Hamamatsu) using Live Acquisition 2.6 software (FEI) for uncaging and EA.hy926 cells response experiments. Monochromatic light source was a Polychrome IV (Till Photonics, Germany) for photochromic ligand experiments.

6.6 Electrophysiology

All the experiments were conducted at room temperature. Transfected and non-transfected HEK293 cells were seeded on glass cover slips the day before the experiments. After 24h cover slips were transferred into a cell bath on an inverted Axiovert 200 microscope (Zeiss). As an excitation source Oligochrome (Till Photonics) was used. Transfected cells were identified by fluorescent after illuminated with 430 or 500 nm wavelength. Whole cell voltage-clamp and current-clamp experiment were performed using Axopatch 200B amplifier (Molecular Devices) connected with a Digidata-1440A Digitizer (Axon Instruments). Signals were low-pass filtered at 2 kHz and digitized with 8 kHz. Application of linear voltage-ramp protocols ranging from -130 to +80 mV (holding potential 0 mV) was controlled by Clampex 10.4 (Axon Instruments) software. Current densities at -90 and +70 mV were plotted against time and normalized by capacitance. Current-voltage relationships from -130 to +80 mV were normalized by capacitance. For neural activity, neurons with -50 to -70 mV resting membrane potential were selected. During the measurement cells were kept in 20 μM CNQX (Tocris) and 50 μM picrotoxin (Sigma Aldrich). For photopharmacological measurements in HEK293 cells illumination was switched every 10 s between UV (365 nm) and blue (430 nm) light for neurons light was being changed every 30 seconds.

For voltage-clamp extracellular solutions contained: 140 mM NaCl, 10 mM HEPES, 5 mM EGTA, 10 mM Glucose, 2 mM $MgCl_2$, 2 mM $CaCl_2$, pH adjusted to 7.4 with NMDG. Pipette solution contained: 120 mM cesium methanesulfonate, 20 mM CsCl, 15 mM HEPES, 5 mM $MgCl_2$, 3 EGTA, titrated to pH 7.3 with CsOH.

For current-clamp pipette solution contained: 120 mM D-Gluconic acid potassium salt, 10 mM HEPES, 5 mM EGTA, 3.5 mM NaCl, 1.5 mM $CaCl_2$, 1.5 mM D-Gluconic acid sodium salt, 0.25 mM $MgCl_2$, titrated to pH 7.3 with KOH. Extracellular solutions contained: 140 mM NaCl, 20 mM Glucose, 10 mM HEPES, 3 mM KOH, 2 mM $CaCl_2$, 2 mM $MgCl_2$, 2 mM NaOH, pH adjusted to 7.4 with NaOH or KOH. Thick-wall patch pipettes from borosilicate glass with filament (Harvard Apparatus) were pulled to a resistance of 10-20 MΩ.

6.7 Statistics

Data analysis and graphical display were performed using Clampfit 10.4 (Axon Instruments), OriginPro 9.1 (OriginLab) and SigmaPlot 13.0 (Systat Software Inc.). Data are presented as mean values ± S.E.M. Primarily, a Shapiro-Wilk test was conducted to test for normality of the value distribution. Whenever normal distribution criterion was met, we used *Student's two-sample t-test* or paired *t-test* to analyse the statistical significance. Otherwise, in case of non-normally distribution, *Mann-Whitney rank sum test* was applied. For groups larger than 3, we used *one-way ANOVA* analysis with subsequent Turkey *post-hoc* test to determine statistical significance. *Chi-square test* was used to analyse responses in cell populations in siRNA knockdown experiments. In general, differences were considered significant at $p<0,05$ and indicated for individual comparisons in figures (* $p<0,05$, ** $p<0,01$, *** $p<0,001$).

7. Results

7.1 Optopharmacological control of TRPC channels by coumarin-caged lipids is associated with a phototoxic membrane effect (*Tiapko et al., 2016*)

7.1.1 Photouncaging of 1,2-DOG induces Ca^{2+} changes in TRPC3 overexpressing HEK293 cells

The lipid sensing machinery of TRPC3 channels represents a unique feature, which stayed enigmatic for many years. Light-controlled lipids may provide an advantage in spatiotemporal control over TRPC channels and allow studying their activity with high precision. Caged lipids have an advantage due to the largely unmodified structure of the released agonist and exert their activating interaction with the target in a way completely dependent on light. Nadler et al. showed that coumarin caged 1,2-DOG (Bhcmoc-1,2-DOG) was effective to generate a Ca^{2+} responses in HELa cells after UV irradiation-induced uncaging. For evaluation of Bhcmoc-1,2-DOG efficiency to induce Ca^{2+} concentration changes in the cytoplasm, HEK293 cells were transfected to express a genetically encoded red-emitting (R-GECO) Ca^{2+} sensor molecule, which does not interfere with coumarin emission, in the presence of YFP-TRPC3. Prior to Ca^{2+} imaging experiments, cells were preincubated with Bhcmoc-1,2-DOG (30 μM) for 10 min, then washed with Tyrode's buffer and mounted in imagine chamber with 2 mM Ca^{2+} containing Tyrode's buffer. Photouncaging was induced by two boosts of UV illumination (340 nm) for 10 s duration. TRPC3-expressing cells co-transfected with R-GECO sensor (TRPC3 overexpressing HEK293 cells) responded with transient fluorescence elevation ($F/F0_{max}$=2.2±0.12), which reported Ca^{2+} changes in the cytoplasm in response to UV-induced photorelease of caged 1,2-DOG (**Figure 2A**). Control HEK293 calls (HEK293 cells) with essentially low endogenous TRPC3 expression and transfected with R-GECO alone, did not exhibit significant Ca^{2+} reaction ($F/F0_{max}$=1.07±0.01; **Figure 2B**) in response to photouncaging of 30 μM of coumarin-caged 12-DOG. Commonly, for activation of TRPC3 channels, higher

concentrations of lipid species are used (8). Therefore, we determined the effect of 100 μM of coumarin-caged 1,2-DOG. At this concentration, we still observed a transient Ca^{2+} increase in response to uncaging of 100 μM Bhcmoc-1,2-DOG in TRPC3-expressing cells ($F/F0_{max}$=3.2±0.09; data not shown). Additionally, we performed experiments with the non-specific blocker of receptor-mediated Ca^{2+} entry pathways SKF 96365, which as well targets TRPC channels (28,31). Transient responses to both Bhcmoc-1,2-DOG concentrations (30 and 100 μM) in YFP-TRPC3 overexpressing cells were efficiently inhibited ($F/F0_{max}$=1.3±0.02) by SKF 96365 (50 μM; **Figure 2**) (29).

To sum up, photouncaging of 1,2-DOG showed specificity to target TRPC3 channels and efficiency to induce cytosolic Ca^{2+} level changes. Consequently, we continued a more detailed characterization of the uncaging response on TRPC3 channels (29).

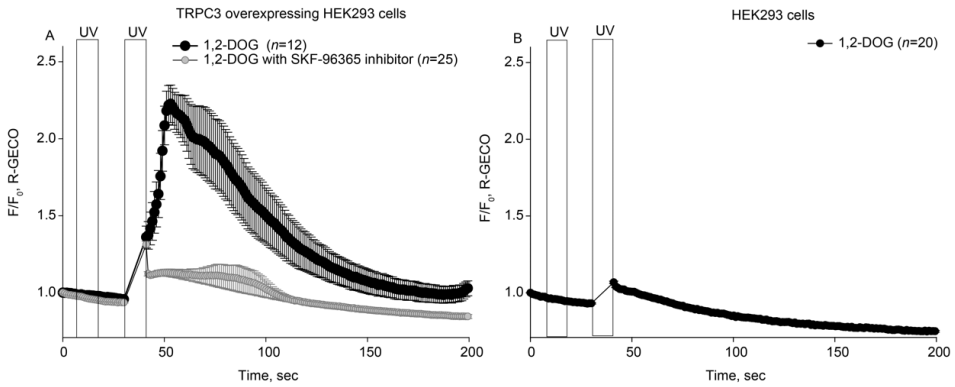

Figure 2. Live-cell imaging of photouncaging-induced changes in Ca^{2+} within HEK293 cells using a genetically encoded red-emitting Ca^{2+} sensor (R-GECO). A, Ca^{2+} transient during phototriggered uncaging of 1,2-DOG (2×10 s, 340 nm, as indicated by UV) in TRPC3 overexpressing HEK293 cells (black line, *n*=12). Inhibition of 1,2-DOG induced Ca^{2+} entry by using 50 μ mol L^{-1} SKF 96365 (grey line, *n*=25). B, Ca^{2+} transient during phototriggered uncaging of 1,2-DOG (2×10 s, 340 nm; UV) in wild type HEK293 cells (*n*=20). Normalized intensity changes (mean±SE) are plotted as a function of time ("Reproduced from **(29)** with permission of publisher Science China Life Sciences, Springer Nature Switzerland, 2016" (https:// creativecommons.org/licenses/by/4.0/)).

7.1.2 Photorelease of coumarin-caged 1,2-DOG triggers non-specific currents independent of TRPC3 expression in HEK293 cells

We observed that a caged DAG efficiently induced Ca^{2+} fluctuations in cells in TRPC3-dependant manner. The next step was to detect and characterize the ability of coumarin-caged 1,2-DOG to induce a cation conductance through TRPC3 channels. Currents were recorded in non-transfected (HEK293 cells) and YFP-TRPC3-transfected (TRPC3 overexpressing HEK293 cells) cells after 1,2-DOG photouncaging. As in Ca2+ imaging experiments, both cells types were preincubated for 10 min in 30 μM and 100 μM of Bhcmoc-1,2-DOG, then washed with external buffer, mounted into a patch-clamp chamber with Bhcmoc-1,2-DOG-free external buffer and voltage-clamped in whole-cell configuration. Holding level of membrane potential was set to 0 mV, and basal currents were elicited with simple 1 sec voltage ramp protocol from -130 mV to +80 mV. Two UV boosts (340 nm, 10 sec) were

applied during the recording at 60 sec and 90 sec time points respectively. A small change in membrane conductance was observed immediately after photorelease of 30 µM Bhcmoc-1,2-DOG with the first UV application which, interestingly, was just augmented by the following second boost (**Figure 3A**). The currents recorded after the first and second UV light illuminations were, however, not resembling TRPC3-specific IV relation and lacked the typical transient time course as elicited by direct diacylglycerol bath application (**Figure 3B**). Consistently, elevating the concentration of the caged lipid to 100 µM increased this "non-transient" current in TRPC3 overexpressing HEK293 cells. To block the UV light-induced currents, we incubated cells with two non-selective cation channel blockers, but the photoinduced conductance were insensitivity to SKF96365 (50 µM; **Figure 3A**) or Ruthenium Red (10 µM; not shown). TRPC3 channels were described as Ca^{2+} dependent channels (32). We performed further experiments in nominally Ca^{2+} free conditions (0 mM) and normal sodium concentration (140 mM). As expected, removal of Ca^{2+} resulted in increased inward current in TRPC3-overexpressing HEK293 cells compared to control cells (-23.1±1.6 pA/pF to -8.7±2.6 pA/pF; **Figure 3C**). However, the recorded currents were still not exhibiting the typical I-V relation of TRPC3 channels. Inward currents recorded in TRPC3-expressing and wild-type HEK293 cells were comparable in amplitude. With application of the unspecific, voltage-dependent Ca^{2+} channel blocker Ruthenium Red (10 µM; **Figure 3C**) we were finally able to isolate and quantify the TRPC3 contribution to the photoreleased conductance. Nevertheless, we clearly demonstrate a light-induced conductance in wild type (control) HEK293 cells representing a TRPC3-independent membrane conductance (**Figure 3D**) (29).

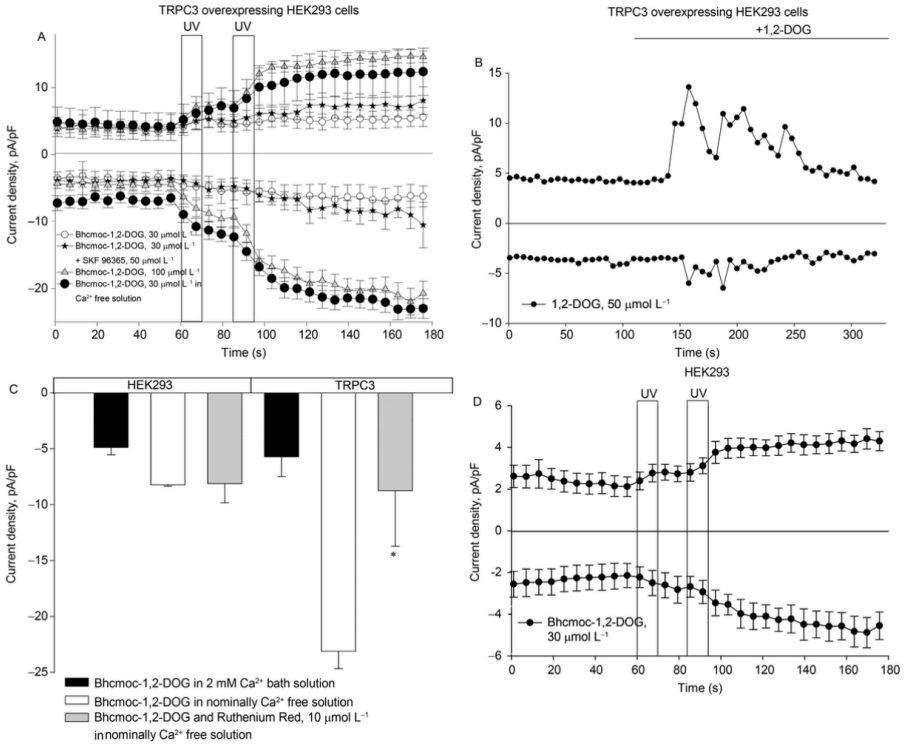
TRPC3 overexpressing HEK293 cells
A
UV
UV
Current density, pA/pF
Time (s)
Bhcmoc-1,2-DOG, 30 μmol L⁻¹
Bhcmoc-1,2-DOG, 30 μmol L⁻¹ + SKF 96365, 50 μmol L⁻¹
Bhcmoc-1,2-DOG, 100 μmol L⁻¹
Bhcmoc-1,2-DOG, 30 μmol L⁻¹ in Ca²⁺ free solution
TRPC3 overexpressing HEK293 cells
+1,2-DOG
B
1,2-DOG, 50 μmol L⁻¹
C
HEK293
TRPC3
Bhcmoc-1,2-DOG in 2 mM Ca²⁺ bath solution
Bhcmoc-1,2-DOG in nominally Ca²⁺ free solution
Bhcmoc-1,2-DOG and Ruthenium Red, 10 μmol L⁻¹ in nominally Ca²⁺ free solution
D
HEK293
Bhcmoc-1,2-DOG, 30 μmol L⁻¹

Figure 3. Patch-clamp characterization of photouncaging-induced changes in membrane conductances of wild type and TRPC3 overexpressing HEK293 cells. A, Average time courses of current recordings in TRPC3 overexpressing HEK293 cells in the presence of Bhcmoc-1,2-DOG (30 μM; n=10, open circles), Bhcmoc-1,2-DOG (100 μM; n=8; grey triangles), Bhcmoc-1,2-DOG (30 μM) and SKF 96365 (50 μM; n=10, black stars), Bhcmoc-1,2-DOG in nominally Ca^{2+} free solution (30 μM; n=4, black circles). **B,** Representative current recording in TRPC3 overexpressing HEK293 cells during bath application of 1,2-DOG (50 μM; n=4). **C,** Bar chart illustrating average inward current densities (-90 mV) determined in control HEK293 cells and TRPC3 overexpressing HEK293 cells after photouncaging (340 nm, 2×10 s) of Bhcmoc-1,2-DOG (30 μM) in 2 mM Ca^{2+} (black bar) and in nominally Ca^{2+} free bath solution (empty bar). Ruthenium Red (10 μM; gray bar) was applied on top of Bhcmoc-1,2-DOG-induced current in nominally Ca^{2+} free bath solution. The current density was calculated at 160 (empty bar) and 205 (gray bar) seconds. The asterisk indicates statistically significant differences ($P< 0.05$) between current density before and after Ruthenium Red application in nominally Ca^{2+} free bath solution. **D,** Average time courses of currents recorded in wild type HEK293 cells in the presence of Bhcmoc-1,2-DOG (30 μM; n=7). Data presented as mean±SE ("Reproduced from **(29)** with permission of publisher Science China Life Sciences, Springer Nature Switzerland, 2016" (https://creativecommons.org/licenses/by/4.0/)).

7.1.3 Photoreleased coumarin 1a exerts a profound effect on the plasma membrane

Coumarin derivatives are used as photosensitizers in medical practice (33). Therefore, we hypothesized that the Bhc-coumarin cage (**Figure 4: coumarin 1a**) once released by uncaging illumination can exert an off-target, side-effect. This concept was tested by incubation of YFP-TRPC3-transfected and widl-type HEK293 cells with coumarin and coumarin derivatives (30 μM; **Figure 4D**) for 10 min and then removed excess of coumarin by a wash with external buffer. Cover slips were mounted into a patch-clamp chamber with coumarin-free external buffer. Current-to-voltage relations recorded in TRPC3-transfected cells incubated with coumarin derivatives (**Figure 4D:1a-1c**) resembled that previously observed after Bhcmoc-1,2-DOG uncaging (**Figure 4B**). Photostimulation of coumarin derivatives (**Figure 4D:1a-1c**) elicited non-specific currents in control HEK293 cells (**Figure 4C**) similar to those observed in transfected cells. These experiments strongly indicate that the light-activated currents initiated by photouncaging of the Bhcmoc-1,2-DOG were for its

major part neither tiggered by the lipid mediator nor reflected the opening of TRPC3 channels. It appears important to note that photostimulation of cells, which were not exposed to coumarin derivatives (DMSO 0,1% only; **Figure 4C**) or loaded with 4-hydroxymethyl coumarin core **1d** (**Figure 4C-D**) that does not absorb UV light, lacked this membrane conductance. Although a minor component of the Bhcmoc-1,2-DOG-induced TRPC3 current was indeed detected (**Figure 4B**), TRPC3 conductance was strongly mimicked by the background current evoked by coumarin derivatives (**1a-c**) photoreactivity (29).

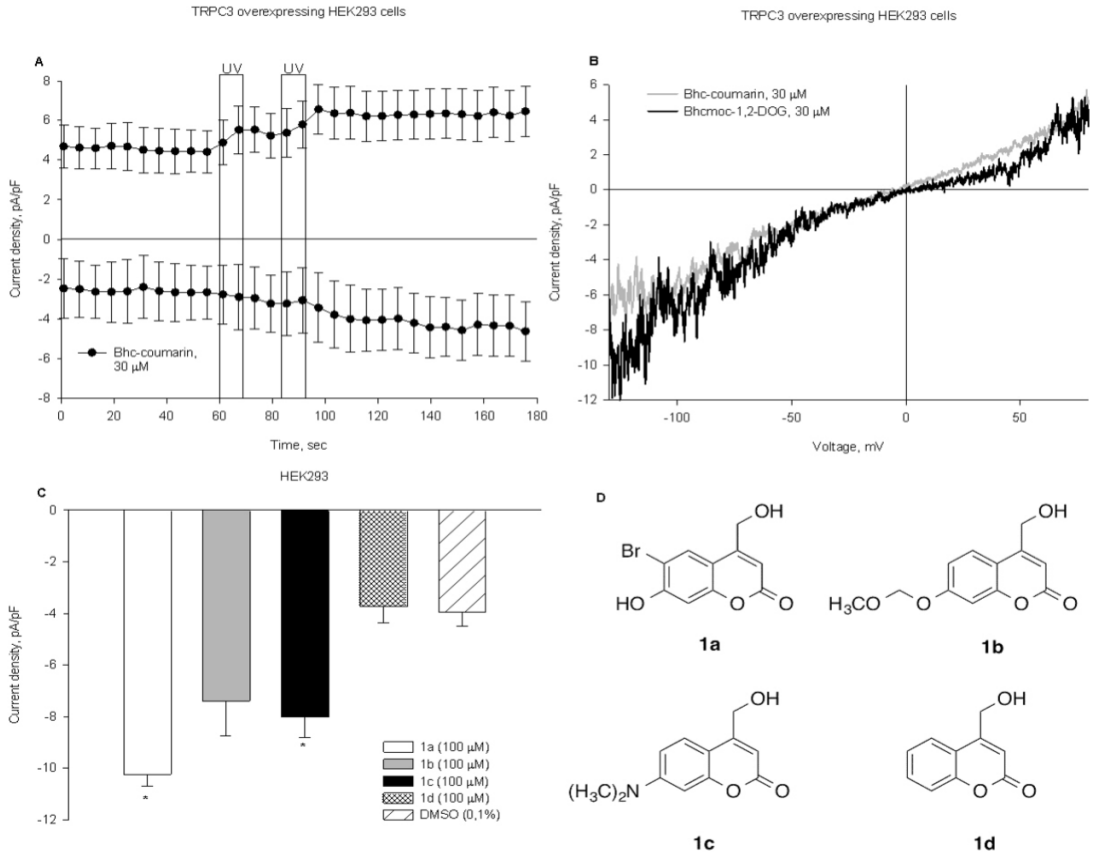

Figure 4. Substituted coumarins cause phototoxicity, which gives rise to a non-selective membrane conductance independent of TRPC3 expression. a, Average time courses of current recordings in TRPC3 overexpressing HEK293 cells treated with coumarin **1a** (30 μM; *n*=5). **b,** Representative current to voltage relation for the "net" light-induced membrane conductance evoked in TRPC3 overexpressing HEK293 cells in the presence of Bhcmoc-1,2-DOG (30 μM; black line) and Bhc-coumarin **1a** as a control (30 μM; grey line). **c,** Bar chart illustrating average inward peak current

densities (-90 mV) of control HEK293 cells induced with Bhc-coumarin (1a; 100 μM; *n*=10), coumarin 1b (100 μM; *n*=10), coumarin **1c** (100 μM; *n*=4), coumarin 1d (100 μM; *n*=5) and dimethyl sulfoxide (DMSO) 0,1% after stimulation with UV light (340 nm, 2×10 s). The asterisks denote statistically significant differences *versus* the response obtained in control HEK293 cells in the presence of coumarin **1a, 1c** and **1d** (4-hydroxymethyl coumarin) was used as a control. D, The structures of various substituted 4-hydroxymethyl coumarin derivatives. Data presented as mean±SE ("Reproduced from **(29)** with permission of publisher Science China Life Sciences, Springer Nature Switzerland, 2016" (https:// creativecommons.org/licenses/by/4.0/)).

7.2 An optically controlled probe identifies lipid-gating fenestrations within the TRPC3 channel (*Lichtenegger M. and Tiapko O. et al., 2018*)

7.2.1 A novel light-sensitive DAG enables precise control over TRPC3 channels activity

Considering the off-target-effect of caged lipids, we switched to photochromic ligand approach as an alternative for photopharmacological targeting of TRPC3. To employ this strategy and examine the lipid gating processes in TRPC3 channels, we first synthetized PhoDAG-1, a recently introduced photoswitchable analog of 2-O-arachidonyl-1-O-stearoyl-sn-glycerol (1,2-SAG) (34) (**Figure 5a**) and tested its suitability for the control of TRPC3 channels by light. In dark and visible light (blue; 430 nm) the azobenzene moiety holds PhoDAG-1 predominantly in a *trans*-state, which was shown as biological inactive (34). We incubated cells with *trans*-PhoDAG-1 (400 µM; **Figure 5c-d**) before the recording and kept cells in the dark until activating illumination (UV; 365 nm) was applied. UV light immediately induced TRPC3-like currents in transfected HEK293 cells but had no effect on control (wild-type or sham transfected?) cells in presence of PhoDAG-1 (control; **Figure 6.**). Current amplitude induced by photoconversion of PhoDAG-1 was relatively small as compared to the response typically induced by DAGs produced after muscarinic receptor stimulation in recombinant TRPC3 channels. The biological activity of DAGs appears dependent on the degree of fatty acid saturation (8). Therefore, we synthetized and tested a modified DAG , which contains two azobenzene-modified side chains resembling two arachidonyl chains (OptoDArG (**Figure 5b**)) (14). General features of photoconversion of OptoDArG resembles that of PhoDAG-1 (34): dark and blue wavelength (430 nm) keeps photoswitchable lipid in *trans*-conformation, while UV (365 nm) rapidly produces *cis*-OptoDArG. We did not observe any significant effect of *trans*-OptoDArG (30 µM) on basal activity of TRPC3 channels overexpressed in HEK293 or non-transfected HEK293 cells (**Figure 6.**). Photoconversion of OptoDArG with UV illumination produced a rapid elevation of TRPC3 activity in transfected HEK293 cells and the amplitude of the current was comparable to a PLC-mediated

response in this cell system. The *cis*-state of OptoDArG was eliciting a conductance with double rectification, representing a fingerprint of TRPC3 channels in transfected HEK293 cells (**Figure 5d**), and had no effect on wild-type HEK293 cells (**Figure 6.**). OptoDArG allowed the efficient and temporally precise optical control over TRPC3 channels (**Figure 5c-d**). We also confirmed efficiency of OptoDArG to trigger PKCα translocation as previously shown for PhoDAG-1 (34). OptoDArG (30 µM) in *cis*-form induced by UV illumination caused a complete PKCα translocation from the cytosol to the plasma membrane within 1 min (**Figure 7**) (14).

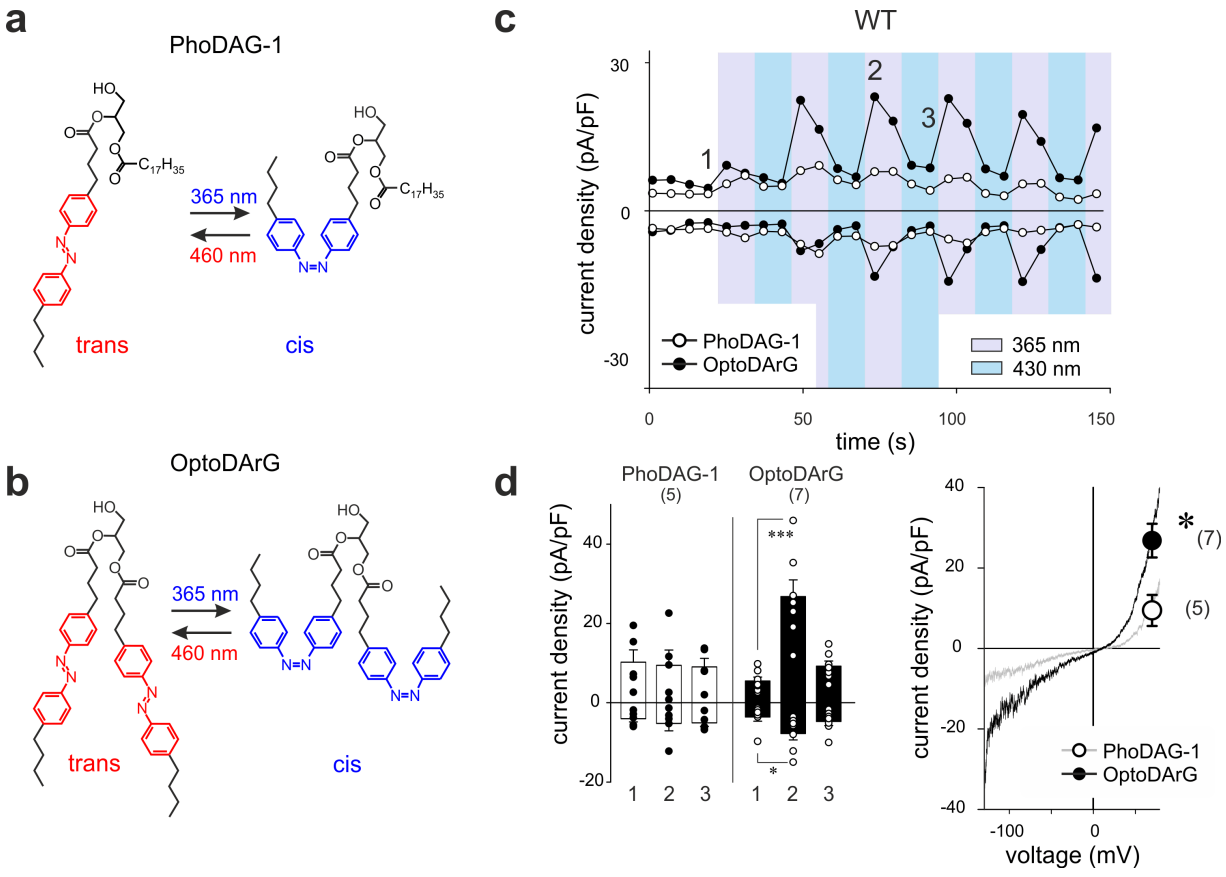

Figure 5. Optical control of TRPC3 conductances expressed in HEK293 cells by DAG photoswitches. a,b, Chemical structures of photoswitchable DAGs: PhoDAG-1 (**(34)**; **a**) and the newly synthesized OptoDArG (**b**). **c,** Representative time courses of the TRPC3-WT conductances recorded at −90 mV and +70 mV during repetitive photoconversion of PhoDAG-1 (400 µM, open circles) and OptoDArG (30 µM, closed circles). UV (365 nm; violet) and blue light (430 nm; blue) irradiation are indicated, with each pulse maintained for 10 s. Time points corresponding to mean

values given in d for basal (before illumination (1), activation (2) and deactivation (3) are indicated. **d, Left panel,** current densities induced by photoconversion of PhoDAG-1 (400 µM, white) and OptoDArG (30 µM, black) are shown for TRPC3-WT (at −90 mV and +70 mV; mean ± S.E.M. are shown; N = numbers of cells measured, indicated in parentheses) at time points given in c; two-tailed t-test or Mann–Whitney rank sum test were applied and significant difference at *P < 0.05; **P < 0.01; ***P < 0.001 are indicated; if no P value is given, comparison with basal (1) current levels is not significant. Induced currents were obtained by voltage-ramp protocols measured at -90 mV and +70 mV under UV (cis photoconversion) and blue light irradiation (trans photoconversion). **Right panel,** representative current to voltage relations of the PhoDAG-1 and OptoDArG-individual values are shown for each of the columns (circles). (N = number of cells measured, indicated in parentheses; corresponding to left panel) for PhoDAG-1 (open circle) and OptoDArG (closed circle); data presented as mean current densities ± S.E.M; *P = 0.016 (“Reproduced from **(14)** with permission of publisher Nature Chemical Biology, Springer Nature Limited, 2018” (https:// creativecommons.org/licenses/by/4.0/)).

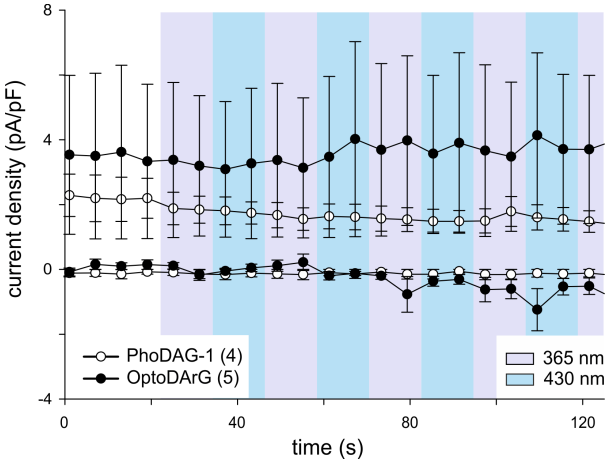

Figure 6. Optical control of DAG photoswitches does not produce any significant membrane conductances in WT HEK293 cells. Time course of membrane conductances generated in WT HEK293, recorded at -90 mV and +70 mV during repetitive photoconversion of PhoDAG-1 (400 µM, open circles) and OptoDArG (30 µM, closed circles). UV (365 nm; violet) and blue light (430 nm; blue) irradiation are indicated, with each pulse maintained for 10 s. Mean values ± SEM are given (N = number of cells are indicated) (“Reproduced from (14) with permission of publisher Nature Chemical Biology, Springer Nature Limited, 2018” (https:// creativecommons.org/licenses/by/4.0/)).

For further identification of the primary lipid-sensing domain and amino acid residues in TRPC3 channels, we combined a structure-guided mutagenesis approach

with the advantages provided by photopharmacological tools. Previously, hydrophobic interactions for TRP family members were identified directly in the pore complex in close proximity to selectivity filter of the channels (35). Hence, we assumed that lipid-protein interactions may occur in lipid-filled cavities within the pore structure of TRPC3 channels. Therefore, we screened TRPC3 sequence and compared it to other members of TRPC family to identified residues potentially exposed to lipids in surrounding plasma membrane (**Table 1, Figure 8**). (14).

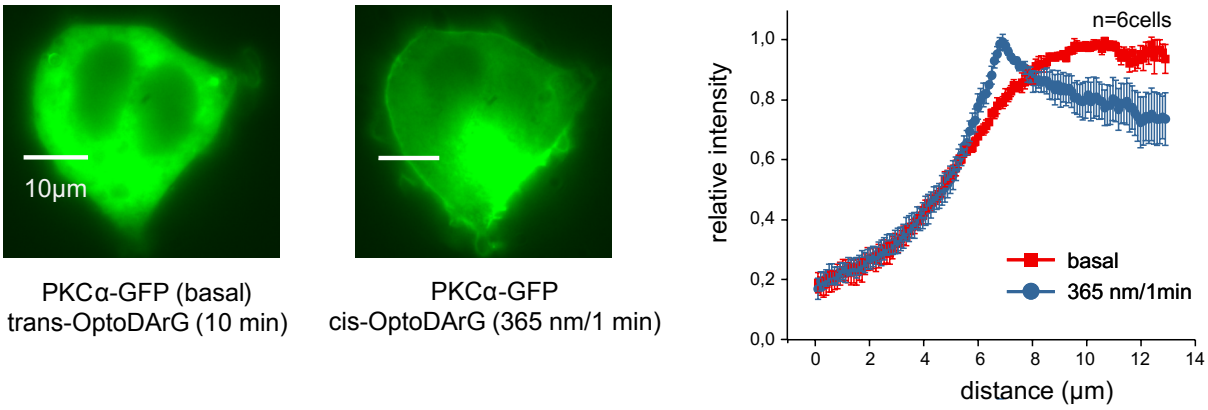

Figure 7. PKCα translocation upon OptoDArG activation. Left panel, Representative PKCα-EGFP fluorescence distribution in a HEK293 (epifluorescence) obtained after 10 min incubation with OptoDArG (30uM) in the dark. PKCα-EGFP was mainly detected in the cytosol. Fluorescence in the nuclei was not observed. Upper right panel: Representative PKCα-EGFP fluorescence distribution in the same cell after 1 min of OptoDArG (30 µM) photoconvertion with UV (100% intensity). **Right panel,** Distribution of the fluorescence intensity of PKCα along the indicated line is shown before (red) and after 1 min (blue) of OptoDArG photoconvertion with UV (100% of intensity). Peak of intensity after photoconversion corresponded to the cell boundary (plasma membrane). Data presented as mean±S.E.M, n = number of cells measured is indicated ("Reproduced from **(14)** with permission of publisher Nature Chemical Biology, Springer Nature Limited, 2018" (https:// creativecommons.org/licenses/by/4.0/)).

7.2.2 G652 is a critical determinant of lipid gating in TRPC3

Mutations in critical regions within the pore complex of TRPC channels like the LFW motif, were shown to effect or eliminate TRPC function (36) presumably by disrupted ligand activation while membrane targeting is preserved. Nonetheless, it is

not clear whether the ligand binding or the permeation pathway is effected. We speculated that, highly conserved regions in the pore complex of TRPC3 channels serve the critical function of lipid recognition and harbor for lipid interaction sites (**Figure 8a)**. From our previous studies employing homology modelling, we identified a key negatively charged residue (E630) as a selectivity filter (37,38). Therefore, we employed structure-guided mutagenesis to screen for a potential lipid-sensing domain within the pore structure of TRPC3 channels (14).

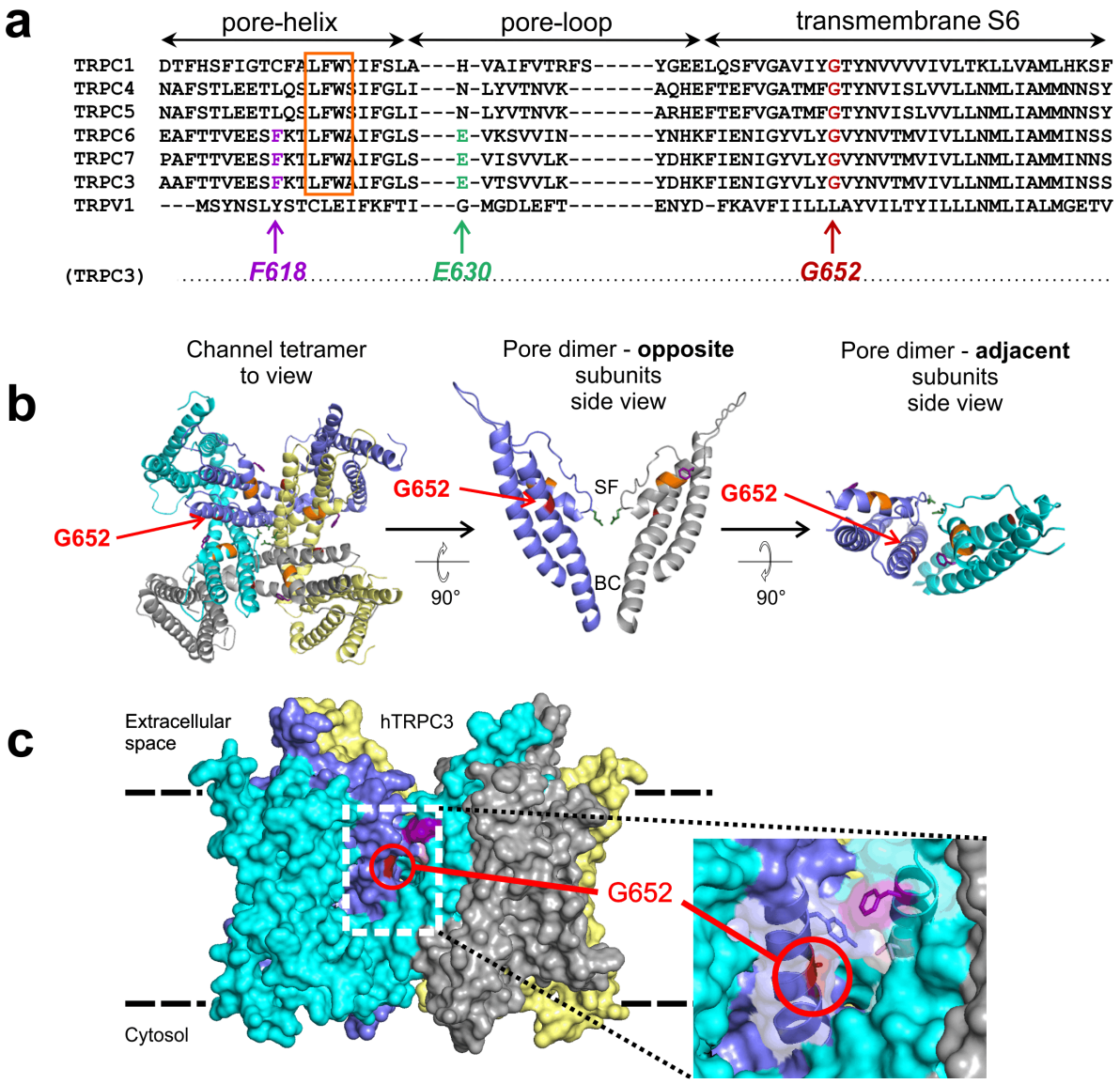

Figure 8. Homology model of human TRPC3 based on the Cryo EM structure of TRPV1 (PDB ID: 3J9J). a, Alignment of conserved residues in regions flanking the TRPC1/3/4/5/6/7 and TRPV1 of pore helix. For TRPC3, G652 (red) and F618 (magenta) and E630 (green) are highlighted along with the LFW motif (orange). Residue numbering corresponds to the human TRPC3 isoform 3. **b, From right to left:** Top view of four subunits forming the tetrameric TRPC3 channel with G652 highlighted. Side view of a section showing the pore-forming transmembrane helices S5-S6 (residue 570 to 674) of two opposite subunits, with the G652 position indicated relative to the selectivity filter (SF) and the S6 bundle crossing gate (BC). Two adjacent chains displaying the subunit interface with a fenestration exposing G652 to the lipid bilayer from the top. **c,** Space filling representation of the 'lipid gating fenestration' within the TRPC3 tetramer assembly from an orthoscopic side view. Figure was done by Barbora Svobodova ("Reproduced from **(14)** with permission of publisher Nature Chemical Biology, Springer Nature Limited, 2018" (https:// creativecommons.org/licenses/by/4.0/)).

By homology modeling, we predicted lateral windows within the pore region behind the selectivity filter exposed to the lipid bilayer responsible for the protein-lipid communication (**Figure 8b/c**). We set an aim to identify residues that are critical for hydrophobic interactions and asses their impact on gating in TRPC3 channels (14).

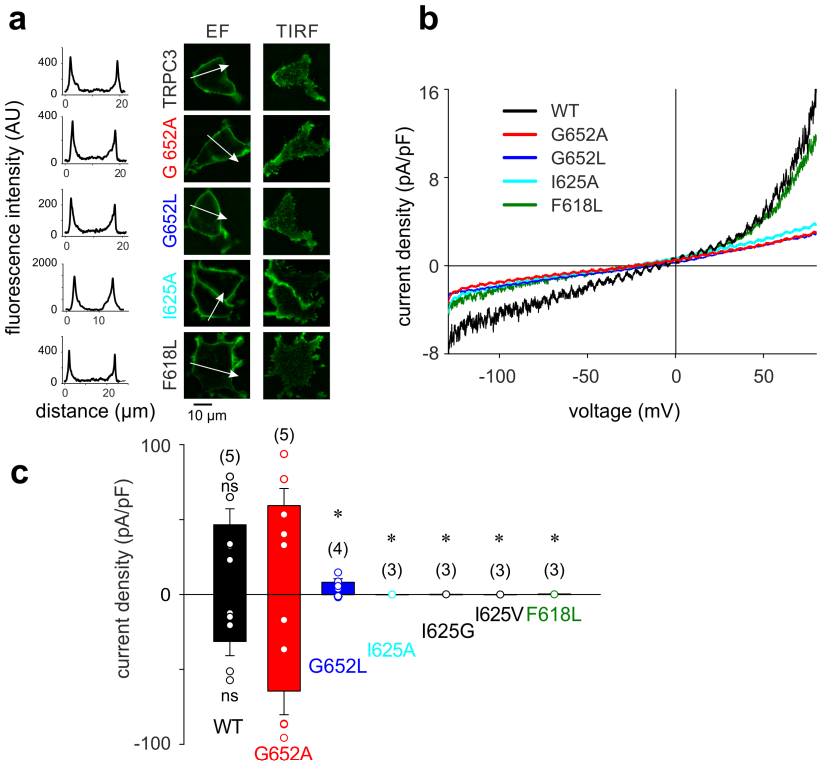

Figure 9. Surface expression, basal activity and GSK sensitivity of TRPC3 mutants. a, Epifluorescence and TIRF images of single cells expressing TRPC3 WT and TRPC3 mutants (G652A; G652L; I625A; F618L). N = number of cells measured > 3 for each of the construct. Cross-sectional profiles of the expression level of TRPC3 WT and TRPC3 mutants in the cell membrane. **b,** Representative basal current recordings in TRPC3 WT (black) and TRPC3 mutants (G652A, red; G652L, dark blue; I625A, cyan; F618L, green). **c,** Mean values of peak response induced by GSK1702934A (10 μM) in TRPC3 WT and TRPC3 mutants (G652A; G652L; I625A; I625G, I625V, F618L). Mean ± SEM, N = number of cells measured is indicated in brackets. * significance at $p < 0,05$. Individual values are shown for each of the data sets (circles) ("Reproduced from **(14)** with permission of publisher Nature Chemical Biology, Springer Nature Limited, 2018" (https://creativecommons.org/licenses/by/4.0/)).

Mutation	Trafficking to the membrane	Basal activity	Agonist sensitivity	
			CCh	GSK
F618L	yes	yes	no	no
I625A	yes	no	no	no
I625G	yes	no	no	no
I625V	no	no	no	no
G652A	yes	yes	reduced	increased
G652L	yes	no	no	reduced

Table 1. Characteristics of mutations in the TRPC3 pore domain

The mutant channels (**Table 1**) were characterized by plasma membrane targeting, preserved basal activity and sensitivity to PLC activation via muscarinic receptor and ability to recognize a novel non-lipid activator (GSK1702934A19/GSK). We identified a few residues, which when mutated retained correct membrane targeting (**Figure 9.**). F618 was suspected to serve a hydrophobic interaction between lipid bilayer and a channel. Interestingly, mutation to alanine (F618A) preserved constitutive activity of the channel, which was comparable to the activity of wild type channels, but activation via both PLC stimulation and GSK were eliminated in the mutant channel (**Figure 9. b/c**). Another interesting site was identified with

position G652 due to the phenotype generated by mutations (G652A and G652L). While G652A retained slight basal activity, it was barely displaying a PLC-induced response or sensitivity to GSK (**Figure 9. c)**. Leucine substitution of glycine in position 652 had a more profound effect: with preserved membrane targeting, mutant channels lacked basal activity and were insensitive to PLC stimulation with significantly reduced GSK response. Both amino acids (F618 and G652) are located within a subunit interaction interface between S6 and the selectivity filter and are opened to hydrophobic interactions with lipids in the plasma membrane. G652 locates directly behind the selectivity filter (**Figure 8**) and due to its conformation freedom expected to allow greater flexibility for gating movements within the pore domain (14). Exchange of G652 to alanine as a less flexible residue resulted in a reduced insensitivity PLC pathway but preserved constitutive activity (**Figure 10. a**). Naturally, larger, bulkier and "more stiff" amino residue leucine in G652L mutant produced almost non-functional channel (**Figure 10. a; Table 1**). Direct lipid activation by SAG (100 µM; **Figure 10. b**) was abolished in the G652A mutant, which suggests a critical role of glycine in this position as lipid recognition determinant. We also noticed that this glycine residue is highly conserved throughout the TRPC family (**Figure 8a**). We mutated the corresponding residue in TRPC6 (G709) to alanine and detected no PLC-mediated activation with preserved GSK sensitivity (**Figure 11.**) (14).

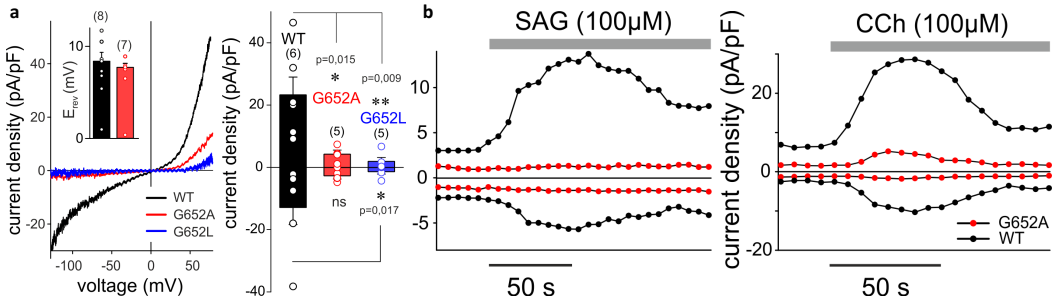

Figure 10. G652 plays a critical role in TRPC3 gating and activation by DAGs. a, Top, Left: Representative I/V-relations of carbachol (CCh)-induced currents (100 µM) through TRPC3-WT (black), G652A (red), or G652L (blue) channels expressed in HEK293 cells. The insert shows the mean reversal potential of currents illustrated in (**a**). **Right:** Histogram displaying mean current densities of CCh-stimulated (100 µM) HEK293 cells, expressing TRPC3-WT (black), G652A (red), or

G652L (blue) channels (right). Data presented as mean ± SEM, number of cells measured indicated above; significant difference shown if p < 0,05. **b,** Representative time courses for current activation by CCh (100 µM, left panel) and SAG (100 µM, right panel) in TRPC3-WT (black) and G652A (red) mutant channels ("Reproduced from **(14)** with permission of publisher Nature Chemical Biology, Springer Nature Limited, 2018" (https:// creativecommons.org/licenses/by/4.0/)).

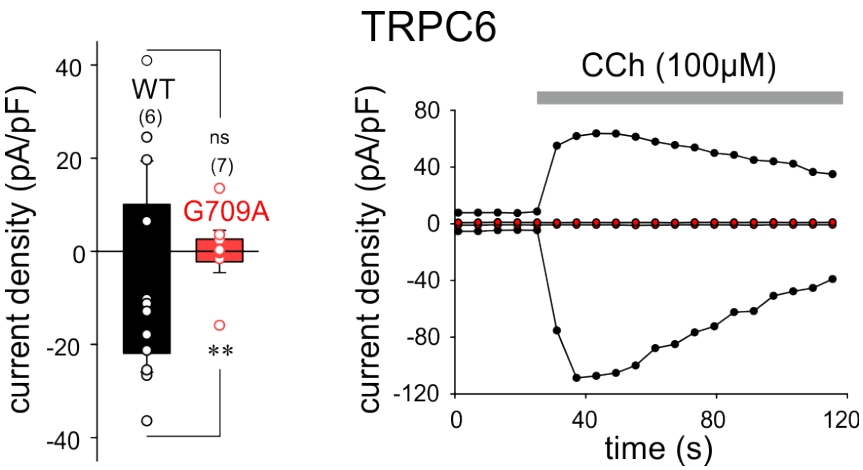

Figure 11. TRPC6 (G709A) displays a similar phenotype as the TRPC3 G652A mutant. Left panel: Histogram displaying mean current densities of CCh-stimulated (100 µM) HEK293 cells, expressing TRPC6-WT (black) and G709A (red) channels. Data presented as mean ± SEM, number of cells measured indicated above; significant difference shown if p < 0,05 ("Reproduced from **(14)** with permission of publisher Nature Chemical Biology, Springer Nature Limited, 2018" (https:// creativecommons.org/licenses/by/4.0/)).

7.2.3 G652 serves recognition of DAGs by TRPC3

As a next consequent step in our investigation, we addressed a question whether G652 determines the ability of TRPC3 to recognize DAG species. We tested and compared the actin of a series of conventional DAGs in order to determine sensitivity of the G652A mutant to lipids. TRPC3-WT channels showed an efficacy order of OAG>SAG>DiC8 (at 100 µM ; **Figure 12.**), which confirmed previously described DAGs sensitivity rankings reported by Hofmann et al (8). Interestingly, this experiment uncovered a general lipid sensitivity of the G652A mutant while its activation preference was clearly changed to DiC8>OAG>SAG (100 µM each; **Figure**

12. b). The G652L mutant displayed general insensitivity to lipids species. Alanine residue (G652A) introduced more rigidity into structure of TRPC3, which resulted in altered ability to discriminate among lipid mediators by the channel (**Figure 12.**) (14).

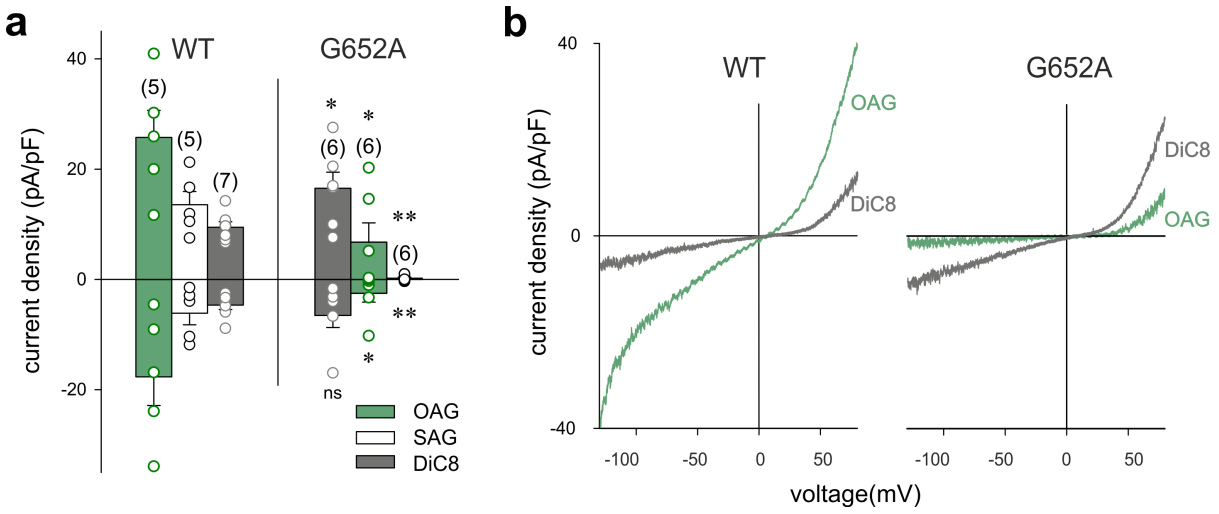

Figure 12. G652A mutation alters discrimination between DAGs by TRPC3. a, Bar chart illustrating current density (at -90 mV and +70 mV) of the maximal responses obtained in TRPC3-WT and G652A induced by OAG (100 μM; green), SAG (100 μM; white) and DiC8 (100 μM; grey). Data presented as mean ± SEM, number of cells measured indicated above; significant difference shown if $p < 0,05$. **b,** Representative I-V relations recorded in TRPC3-WT and G652A after application of OAG (100 μM; green) and DiC8 (100 μM; grey) application ("Reproduced from **(14)** with permission of publisher Nature Chemical Biology, Springer Nature Limited, 2018" (https:// creativecommons.org/licenses/by/4.0/)).

To explain the observed change in lipid sensitivity, we hypothesised that the G652 position may serves as a crucial structural element to allow molecular accommodation of DAG species within the pore complex and may represent part of the lipid sensing machinery of TRPC3 channels (14).

To test the concept, we utilized our newly developed photopharmacological tool OptoDArG and PhoDAG-1. Sensitivity to photocycling of structural the analogue of SAG (PhoDAG-1; 400 μM) was completely abolished in both G652 mutants

(**Figure 13. a**). In contrast, response to light-dependent on/off cycling of OptoDArG (30 μM) in G652A was even facilitated as previously observed for DiC8 (**Figure 12.**). Surprisingly, the corresponding mutation in TRPC6 (G709A) displayed a generally reduced sensitivity at these concentrations of OptoDArG (**Figure 14**) (14).

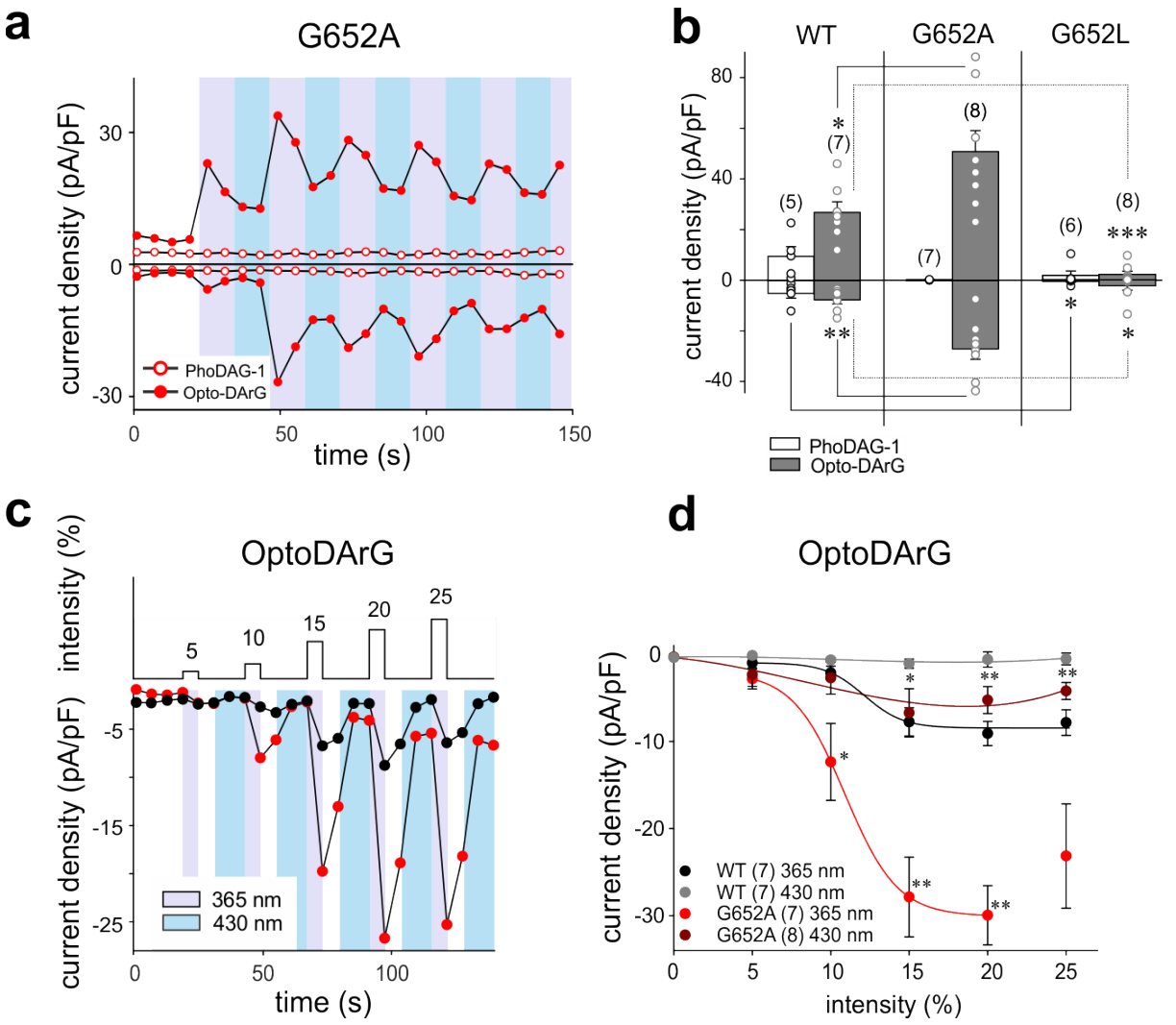

Figure 13. **Photopharmacological comparison of DAG sensitivity in TRPC3-WT and G652A channels reveals altered threshold. a,** Representative time course of the G652A conductance recorded at -90 mV and +70 mV during the repetitive photoconversion of PhoDAG-1 (400 μM, open circles) and OptoDArG (30 μM, closed circles). UV (365 nm; violet) and blue light (430 nm; blue) irradiation is indicated, with each pulse maintained for 10 s. **b,** Current densities (at -90 mV and

+70 mV) at the maximum, net responses induced by PhoDAG-1 (400 µM, white) and OptoDArG (30 µM, grey) are shown for TRPC3-WT and G652A. Number of cells measured indicated above; significant difference shown if p < 0,05. **c,** Representative responses to increasing light intensity (maximal output power 670 mW) of TRPC3-WT (black) and G652A (red) expressing HEK293 cell induced by photoisomerization of OptoDArG (30 µM). UV (365 nm, violet, pulse held for 2 s) and blue light (430 nm, blue, pulse held for 10 s). **d,** Light intensity – current density relation for TRPC3-WT (peak inward current = black; minimum current level during deactivation = grey) and G652A (peak inward current = red; minimum current level during deactivation = deep red) obtained by photoisomerization of OptoDArG (30 µM). Data presented as mean ± SEM, number of cells measured indicated above; significant difference shown if p < 0,05 ("Reproduced from **(14)** with permission of publisher Nature Chemical Biology, Springer Nature Limited, 2018" (https://creativecommons.org/licenses/by/4.0/)).

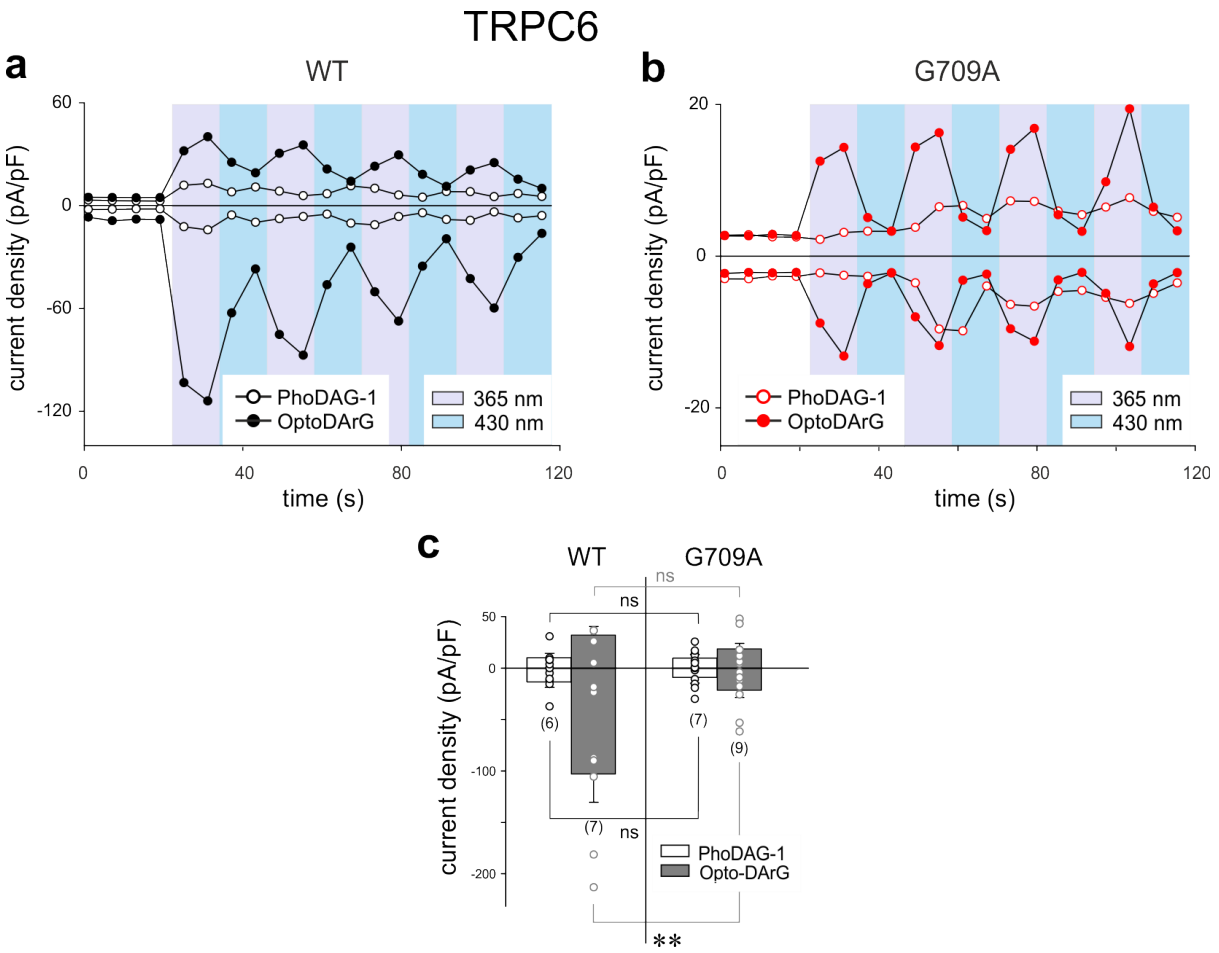

Figure 14. Optical control of TRPC6 conductances expressed in HEK293 cells by DAG photoswitches. Upper panel: Representative time courses of the TRPC6-WT (black) and G709A (red) conductances recorded at -90 mV and +70 mV during repetitive photoconversion of PhoDAG-1 (400 µM, open circles) and OptoDArG (30 µM, closed circles). UV (365 nm; violet) and blue light (430 nm; blue) irradiation are indicated, with each pulse maintained for 10 s. **Lower panel:** Current density (at -90 mV and +70 mV) of the maximum responses obtained with TRPC6-WT and G709A, induced by PhoDAG-1 (400 µM, white) and OptoDArG (30 µM, grey). Data presented as mean ± SEM, number of cells measured indicated above; significant difference shown if $p < 0,05$ ("Reproduced from (14) with permission of publisher Nature Chemical Biology, Springer Nature Limited, 2018" (https:// creativecommons.org/licenses/by/4.0/)).

Interestingly, the ability of OptoDArG to cycle the channel between open and closed states displayed an overall transient response (**Figure 13. A).** The peak currents, obtained at sub-maximum light intensities, resembled the typical time course of a bath application of DAGs (**Figure 10. b**) with fast current development followed by final inactivation/desensitization (14).

It appears important to note that repetitive activation-deactivation of the TRPC3 mutant (G652A) by photoswitching of OptoDArG (30 µM) displayed an incomplete deactivation after switching to biologically inactive *trans*-form, a phenomenon that was less observed in TRPC3-WT channels (**Figure 5c**). This phenomenon was present just upon application of higher light intensities. Therefore, we set out to estimate the threshold of activation for both channels to obtain information on potencies of the light-dependent agonist OptoDArG. To do that, we took advantage of the photopharmacological principle to control the precise quantity of the ligand next to the protein of interest and established a light intensity (quantity)-activity relation for TRPC3 WT and G652A mutant channels by variation of light intensities (**Figure 13. c**). The threshold for G652A mutant activation was significantly lower than that recorded in TRPC3 WT (**Figure 13. d**). Although activation and desensitization were barely noticeable at low light intensities, we cannot exclude an overlap of slower gating processes with rapid photodependent potentiation-inactivation especially at higher concentrations of the active lipid. Thereby, our ability

to precisely delineate maximum responses and potencies was distorted (14). Of note, a moderate elevation of current levels during deactivation was again observed at higher light intensities only in the mutant channel. The fact that basal current levels during deactivation increased in an UV light intensity-dependent manner (**Figure 13. d**) may be explained either by enhanced potency of the lipid activator or by a slowed photoconversion of the photochromic lipid while associated with the mutant (14).

We assumed an altered interaction between subunits may lead to structural rearrangements that interfere also with the sequence of conformational changes required for final channel opening. Such an altered cooperativity may contribute to the observed OptoDArG hypersensitivity in the mutant channel. The alanine mutation in G652 may have two consequences for cooperativity: either changing the number of necessary conformational steps involved or the coupling between these transitions in the channel complex (14). As the photoconversion of azobenzene photoswitches is essentially instantaneous (34,39), we utilized optical advantage of OptoDArG (optical 'lipid-clamp') to characterize the kinetics of the molecular mechanism of lipid recognition and to investigate the mutation-dependent cooperativity change in G652A (14).

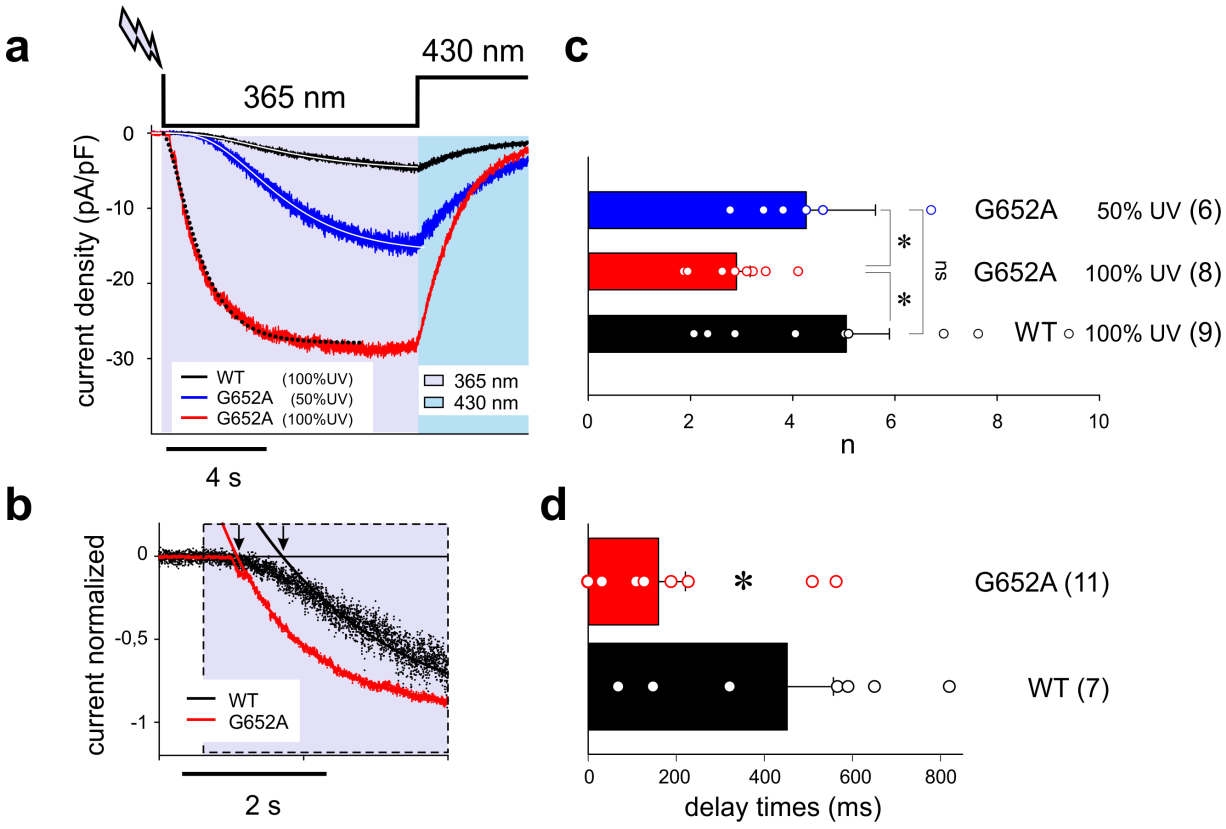

Figure 15. Optical clamp of TRPC3-WT and G652A currents by OptoDArG reveals divergent kinetics and altered cooperativity. a, Representative traces showing the inward currents induced by OptoDArG (30 µM) in a whole-cell, gap-free recording (holding potential: −40 mV, normalized by capacitance) in TRPC3-WT and G652A expressing HEK293 cells. UV (365 nm, violet) and blue light (430 nm, blue). TRPC3-WT (black) and G652A (red) responses were induced with 100% intensity of UV, G652A (blue) was triggered with 50% UV. Exponential fits of current activation for TRPC3-WT (black, 100%) and G652A (red, 100%) and G652A (blue, 50%) are shown. **b,** Exponential fits of initial phase of current activation for TRPC3-WT (black) and G652A (red). Signal was normalized to peak current. **c,** Power (n) of power-exponential fitting is shown (f = A*(1-exp(-x/tau))^n). **d,** Histogram displaying the current activation delay for TRPC3-WT (black) and G652A (red). Data presented as mean ± SEM, number of cells measured indicated above; significant difference shown if p < 0,05 ("Reproduced from **(14)** with permission of publisher Nature Chemical Biology, Springer Nature Limited, 2018" (https:// creativecommons.org/licenses/by/4.0/)).

Currents were monitored at a fairly physiological membrane potential of -40 mV. We took advantage of the exceptional temporal precision of the optical 'lipid-clamp' approach to gain an insight into the activation/deactivation kinetics of TRPC3

WT and G652A mutant channels. Activation (on) kinetics when challenged with OptoDArG showed sigmoid time dependence for both channels. We also performed optical “PhoDAG-1-clamp” in WT but this photolipid was non-effective in activating the mutant channel (**Figure 15 and Figure 16**). Considering the results with PhoDAG-1, we performed further kinetic analysis with OptoDArG only. Sigmoidicity of channel opening by the photochromic mediator OptoDArG clearly indicates a process that requires multiple conformational transitions (**Figure 15a**) (14). Moreover, comparison of sigmoidal fits in WT and mutant channels showed a significant difference in on-kinetics at the same conditions and light intensities. We calculated an actual response of WT and mutant channels to *cis*-OptoDArG by finding an interception between single exponential fit and the start of the illumination switch. Mutant channels responded significantly faster to active OptoDArG (**Figure 15b-d**) (14). Furthermore, we characterized sigmoidicity by power exponential fitting and estimated power (*n*) as an indicator of the gating cooperativity between subunits during the process of channels opening. TRPC3 WT channels displayed a mean *n*=5 at a maximum light intensity (100% UV; **Figure 15c**). Calculated from power exponential fitting of the activation time course we determined *n* for G652A, which exhibited decreased delay of activation, as clearly reduced (*n* = 2.9) at the same level of light illumination (100% UV; **Figure 15c**). At 50% of UV light intensity *n* was moderately but significantly increased to 4,2 in comparison to 100% UV intensity in the G652A mutant. The overall comparison yielded no significant differences regarding time constants for current activation/deactivation kinetics of WT and mutant with slightly reduced ratios of T_{off}/T_{on} for G652A compare to WT channels (**Figure 17**). In summary, our photopharmacological approach reveals a distinctly altered response to OptoDArG in the mutant channel. When G652 was mutated to a more rigid amino residue (Ala) the number of conformational changes in the channel induced by lipid interactions are significantly reduced indicating a significant role of G652 in recognition of the lipid and/ in the lipid-gating process (14,40)

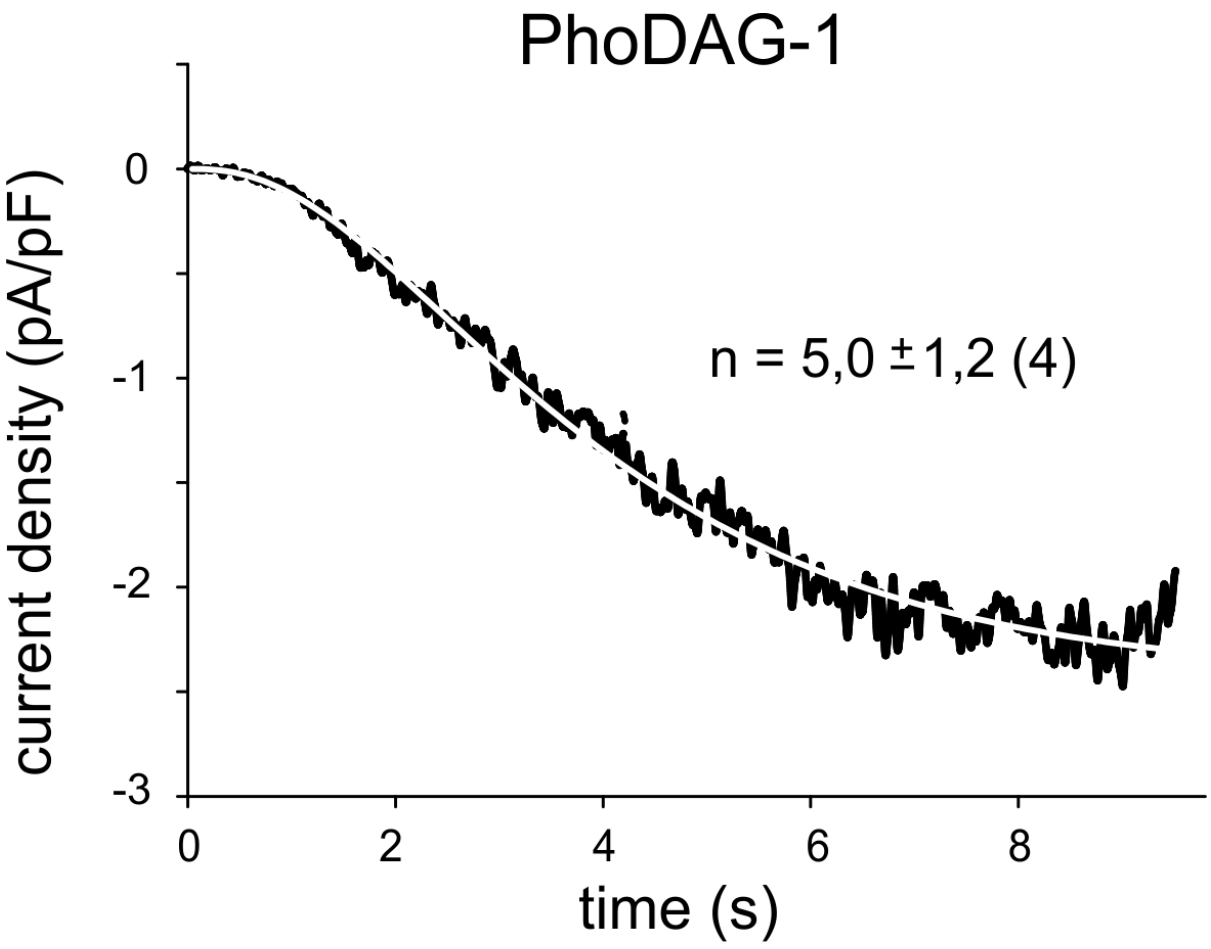

Figure 16. Activation kinetics of TRPC3-WT channel during cis photoconversion of PhoDAG-1 (400 µM). Representative traces showing the inward current (normalized by capacitance) induced by illumination at 365 nm and PhoDAG-1 (400 µM) at a holding potential of −40 mV in TRPC3-WT expressing HEK293 cells. The response was induced with 100% intensity of UV. Exponential fit of current activation and power (n) of power-exponential fitting (f = A*(1- exp(-x/tau))^n) are indicated ("Reproduced from **(14)** with permission of publisher Nature Chemical Biology, Springer Nature Limited, 2018" (https:// creativecommons.org/licenses/by/4.0/)).

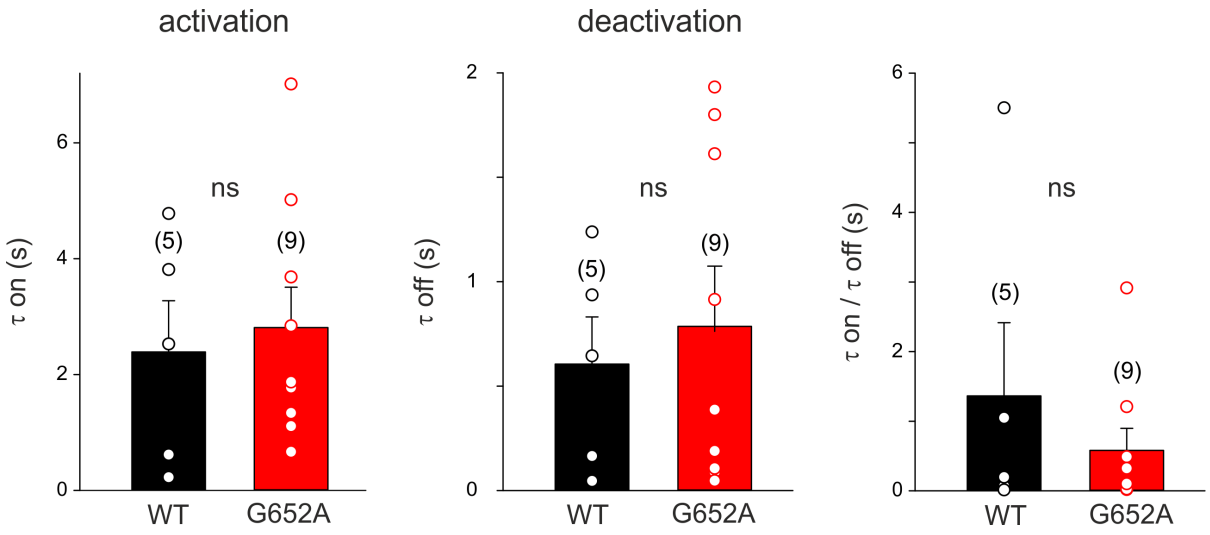

Figure 17. Activation/deactivation delay comparison of G652A mutant and TRPC3 WT in optical 'lipid-clamp' experiments. Time constants for activation (on) and deactivation (off) and ratio of (on/off) kinetics derived by 'lipid-clamp' pulses at -40 mV in TRPC3 WT and G652A with OptoDArG (30 μM). Data presented as mean ± SEM, number of cells measured indicated above; significant difference shown if $p < 0,05$ ("Reproduced from **(14)** with permission of publisher Nature Chemical Biology, Springer Nature Limited, 2018" (https:// creativecommons.org/licenses/by/4.0/)).

7.3 A new small molecule photoswitch for lipid-independent, optical control of TRPC3 channels (*Tiapko O. and Shresta N.et al., under revision*)

The TRPC family has been implicated in a variety of diseases although a comprehensive understanding of their specific role in the complex setting of organ physiopathology is lacking [1-3]. TRPC channels are expressed throughout the human body with particular abundancy in brain and cardiovascular tissues [2]. Our current knowledge about the cell type-specific functions of TRPC molecules, their dependencies on temporal activity pattern and connections with down-stream signaling pathways is incomplete. This paucity of understanding is due to the difficulties encountered when attempting to precisely and specifically manipulate TRPC activity in native tissues. Hence, the development of photopharmacological strategies that target TRPC signaling pathways is needed to make advance to the field.

Azobenzene photoswitches are both suitable and valuable for the high precision control of TRPC channels as has recently been demonstrated by reports on the spatial and temporal precision of TRPC activation achieved with photoconvertible diacylglycerols (29,41,42). Although exceptionally effective in terms of channel activation, this latter approach suffers from two inherent limitations, namely its lack of selectivity and the uncertainty of its dependence on metabolic pathways.

7.3.1 Screening for a potent agonist of TRPC3 channels

Over the past decade, an array of small molecules have been identified, which either inhibit or activate TRPC channels with variable degree of selectivity (24,43-45). Photoswitchable channel blocker do not appear perfectly suitable for efficient TRPC3 photopharmacology since the channels tend to inactivate or desensitize efficiently, and it is barely feasible to exert cyclic current control over cellular Ca^{2+} signaling by blocking and unblocking of a constitutively open TRPC3 pore. We therefore set out to generate a photoswitch based on the structural features of the recently characterized TRPC3 activator GSK1702934A (GSK) (24). This molecule was found to activate native TRPC channel complexes with an apparently high degree of selectivity and

reasonable potency. Notably, GSK acts independently of membrane lipid metabolism, and significant off-target effects on other ion conductances have not yet been detected(24). Based on this knowledge we hypothesized that the creation and manipulation of a GSK-based azobenzene photoswitch might enable us to exert efficient control over cellular TRPC3 signaling.

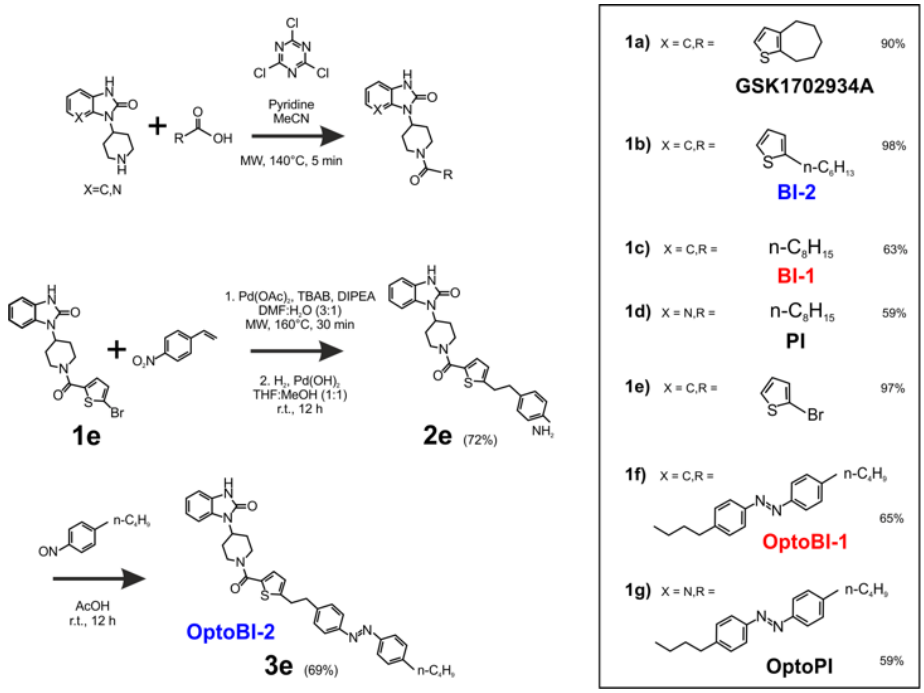

Scheme 1. Synthesis of selected analogues of GSK1702934A (GSK), designated as BI-1, BI-2, PI, and the corresponding photoresponsive derivatives designatred as OptoBI-1, OptoBI-2 and OptoPI. Yield is given in %.

As a first step, we synthetized a few selected GSK-related structures with potential agonist activity in biological activity tests (Scheme 1, Figure 1). The newly synthesized compounds (**Scheme 1b-d**) were easily obtained in good to high yields by employing a synthetic procedure developed earlier (45) and fully characterized by using analytical techniques (see Supporting information for details). The obtained molecules, two different 1,3-dihydro-2*H*-benzo[*d*]imidazol-2-ones (BI-1, BI-2) and one 1,3-dihydro-2*H*-imidazo[4,5-*b*]pyridin-2-one derivative (PI) (**Fig. 18a**) were then

initially compared with GSK in terms of their preserved activity at recombinant TRPC3 channels that were overexpressed in human embryonic kidney (HEK293) cells.

All three compounds activated recombinant TRPC3 channels in whole-cell voltage-clamp experiments. **Fig. 18b** illustrates the comparison of I-V relations among the peak conductances (ramp responses from -130 mV to +80 mV, 1s) induced by GSK, BI-1, BI-2 and PI in HEK293 cells expressing a YFP-TRPC3 fusion construct. At a concentration of 10 µM all compounds transiently induced currents that featured the double-rectifying I-V relation typical of TRPC3 conductances (**Fig. 18b**). Time-courses of the current activation are shown in **Fig. 18c**. The observed transient increase in conductance displayed a time course similar to that initiated by GSK, and peak current densities produced by BI-2 and PI were comparable to those evoked by GSK, whereas BI-1 induced slightly lower responses (**Fig. 18d**).

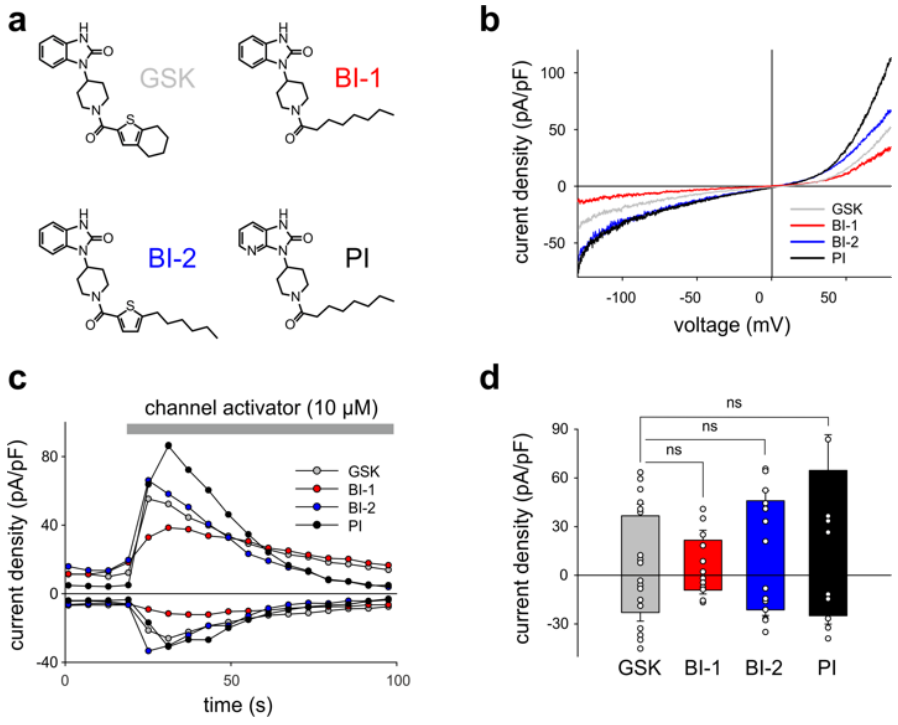

Figure 18. Chemical structures of GSK1702934A (GSK) and GSK derivatives (BI-1, BI-2 and PI). b) Current to voltage relations of the net conductances (I_{max}-I_{basal}) induced by GSK, BI-1, BI-2 and PI (10 µM each) obtained in TRPC3-transfected HEK293 with voltage-ramp protocols. c)

Representative time courses of the TRPC3 conductances recorded at -90 mV and +70 mV during administration of channel activators (GSK, BI-1, BI-2 and PI as indicated) at 10 µM concentrations. d) Current density of net, maximum responses obtained at -90 mV and +70 mV (mean ± SEM). Statistical significance was tested by two tailed t-test (normally distributed values) or Mann–Whitney tests (non-normally distributed values). ns = not significant ($p > 0.05$); N cells: GSK = 9; BI-1 = 6; BI-2 = 7; PI = 5).

7.3.2 Introducing a photoswitchable GSK derivative for optical control over TRPC3 channels

As HEK293 cells essentially express low endogenous levels of TRPC proteins including TRPC3 while expressing other ion channel genes[13-15], the lack of effects observed in non-transfected HEK293 (**Fig. 19e-f**) cells not only demonstrated that the activity of these compounds was strictly dependent on TRPC3 expression, but also indicated a certain degree of TRPC specificity. On the basis of these results, all three compounds were considered as suitable molecular scaffolds for development of photoswitches to control of TRPC3. Next, we generated three corresponding azobenzene derivatives (**Scheme 1 and Figu. 19**), designated as OptoBI-1 (**Scheme 1f**), OptoBI-2 (**Scheme 1e**) and OptoPI (**Scheme 1g)**, which feature efficient *trans-cis-trans* light-triggered photoisomerization (see Supporting information for details). Typically, these azobenzene-photoswitches reside in the thermodynamically more stable *trans*-conformation, while their irradiation with UV light (365 nm) initiates rapid isomerization into the *cis*-form. Triggering the opposite *cis-trans* transition can be rapidly and easily conducted by illuminating the photochromic ligand with visible light (blue, 430 nm).

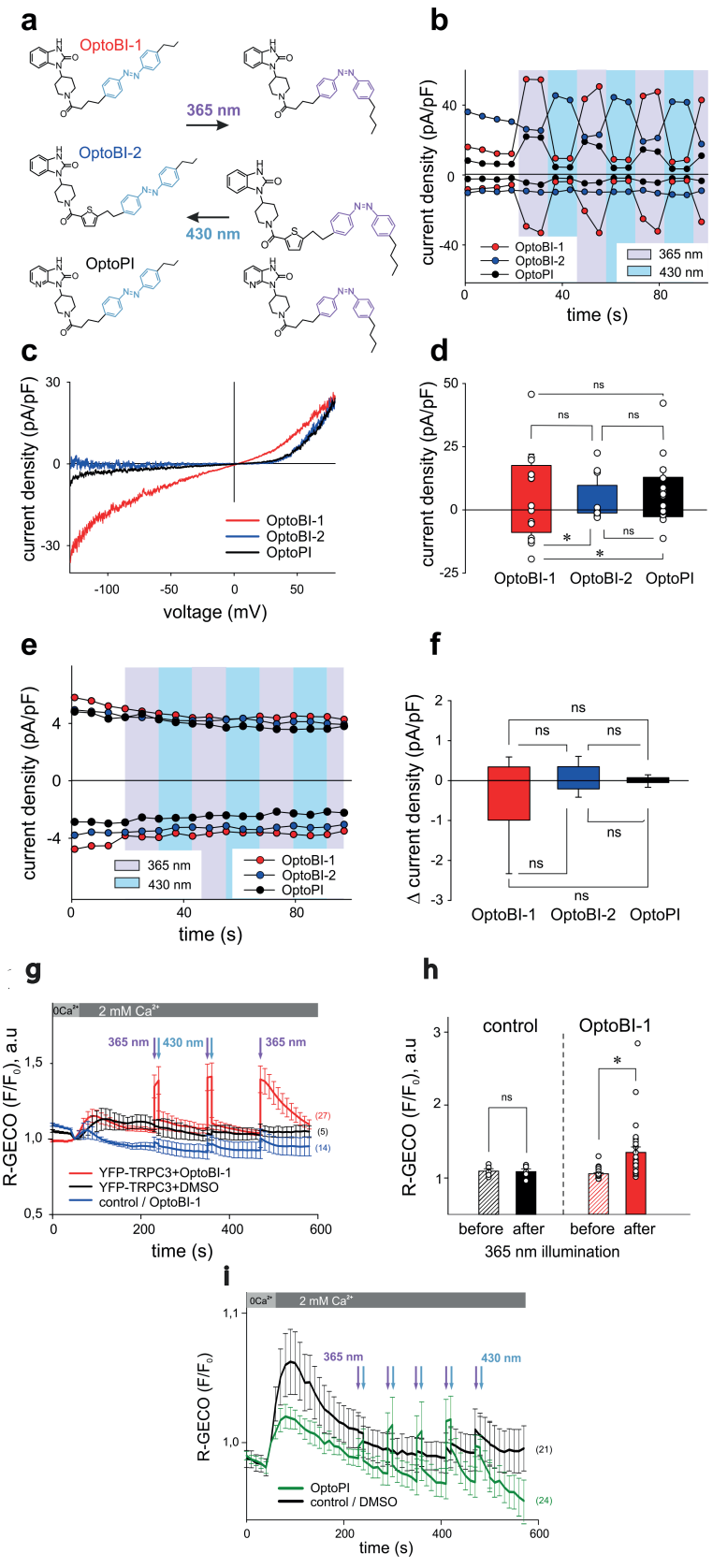
a
OptoBI-1
365 nm
OptoBI-2
430 nm
OptoPI
b
current density (pA/pF)
40
0
-40
OptoBI-1
OptoBI-2
OptoPI
365 nm
430 nm
0
40
80
time (s)
c
current density (pA/pF)
30
0
-30
OptoBI-1
OptoBI-2
OptoPI
-100
-50
0
50
voltage (mV)
d
current density (pA/pF)
50
25
0
-25
ns
ns
ns
ns
*
*
OptoBI-1
OptoBI-2
OptoPI
e
current density (pA/pF)
4
0
-4
365 nm
430 nm
OptoBI-1
OptoBI-2
OptoPI
0
40
80
time (s)
f
Δ current density (pA/pF)
2
1
0
-1
-2
-3
ns
ns
ns
ns
ns
ns
OptoBI-1
OptoBI-2
OptoPI
g
0Ca2+
2 mM Ca2+
365 nm
430 nm
365 nm
R-GECO (F/F0), a.u
1,5
1,0
0,5
(27)
(5)
(14)
YFP-TRPC3+OptoBI-1
YFP-TRPC3+DMSO
control / OptoBI-1
0
200
400
600
time (s)
h
control
OptoBI-1
R-GECO (F/F0), a.u
3
2
1
ns
*
before
after
before
after
365 nm illumination
i
0Ca2+
2 mM Ca2+
365 nm
430 nm
R-GECO (F/F0)
1,1
1,0
(21)
(24)
OptoPI
control / DMSO
0
200
400
600
time (s)

Figure 19. Chemical structures of photoswitchable GSK derivatives. a, OptoBI-1, OptoBI-2, OptoPI; **b,** Representative time courses of the TRPC3 conductances recorded at -90 mV and +70 mV during repetitive photoconversion of OptoBI-1, OptoBI-2 and OptoPI (10 µM). Cells were kept in dark prior to light application, following by cycling of UV (365 nm; violet) and blue light (430 nm; blue) illuminations, applied for 10 s each (indicated). **c,** Representative net I-V relations (I_{max}-I_{basal}) for OptoBI-1, OptoBI-2 and OptoPI-induced (10 µM) obtained in TRPC3-transfected HEK293 cells with voltage-ramp protocols. **d,** Current densities, induced by photoconversion of OptoBI-1, OptoBI-2 and OptoPI (10 µM) at -90 mV and +70 mV; mean ± SEM, N = cells: OptoBI-1 = 8; OptoBI-2 = 5; OptoPI = 10; individual values are included (circles). Statistical significance was tested by two tailed t-test (normally distributed values) or Mann–Whitney test (non-normally distributed values). ns = not significant ($p > 0.05$); *$p < 0.05$; N = number of cells measured. **e,** Representative time courses of the conductances recorded in HEK WT cells at -90 mV and +70 mV during repetitive photoconversion of OptoBI-1, OptoBI-2 and OptoPI (10 µM). UV (365 nm; violet) and blue light (430 nm; blue) illumination, applied for 10 s each are indicated. **f,** Statistics on light-induced current changes (net responses) in cells treated with the indicated photoswitches (mean ± SEM); N (cells) = 4-6. **g,** Time courses of Ca^{2+}-sensitive R-GECO fluorescence during OptoBI-1 (10 µM) photoconversion in TRPC3 plus R-GECO (red and black trace) and R-GECO only (blue trace) expressing in HEK293. Illumination (365 nm; 10 s and 430 nm; 30 s) performed before fluorescence recording, is indicated by arrows (N of cells: YFP-TRPC3 and OptoBI-1 = 27; YFP-TRPC3 and DMSO = 5; HEK293 WT and OptoBI-1 = 14). **h,** Fluorescence levels before and after UV light-induced changes in cells co-transfected with TRPC3 and R-GECO in presence of DMSO (control) or cis-photoconversion of OptoBI-1 and OptoPI (10 µM). Data presented as mean ± SEM, individual values shown as circles; significant difference shown if $p < 0,05$; **i,** Time courses of Ca^{2+} changes during OptoPI (10 µM) photoconversion (green trace) and in DMSO only (black trace) in HEK293 cells co-expressing recombinant TRPC3 plus R-GECO. Illumination (365 nm; 10 s and 430; 30 s) was performed before fluorescence recording and is indicated by arrows (N of cells YFP-TRPC3 and OptoPI = 21; YFP-TRPC3 and DMSO (control) = 24). Parts of the figure (**g-i**) were done by Sonja Lindinger.

The suitability of these photoswitches to control of TRPC3 was tested again in the HEK293 heterologous expression system by patch-clamp recordings. We characterized the activity of the GSK derivatives, OptoBI-1, OptoBI-2 and OptoPI (**Fig. 19a**; at 10 µM) on the basis of the conductance generated by recombinant TRPC3 during the cyclic photoisomerization. The compounds were present in the bath solution while measurements were taken and optical cycling was initiated after about 20 s of control recording (**Fig. 19b**). While OptoBI-1 and OptoPI did not activate

a current in the dark-adapted *trans* conformation, trans OptoBI-2 (before first illumination; **Fig. 19b**), generated constitutive TRPC3 activity. Repetitive conformational cycling initiated by exposure to UV (365 nm) and blue light (430 nm) illumination rapidly changed the TRPC3 conductance in the presence of all three photoswitches. The current inactivation or desensitization that is typically observed with photoswitchable lipids or conventional agonist stimulation(42) was barely detectable with these GSK derivatives using the short-term cyclic activation protocol. UV-induced *cis* isomerization activated the TRPC3 conductance in the presence of OptoBI-1 or OptoPI, but inhibited currents with OptoBI-2. Thus, all three photochromic modulators operated the channel between a basal and an activated state in a light dependent manner, OptoBI-2, however, displayed a reverse dependency on isomerization as compared to its congeners. Interestingly, the efficacy of current activation at 10 µM was highest in the presence of OptoBI-1, which originated from the relatively weak activator BI-1 (**Fig. 18**). Hence the incorporation of the azobenzene moiety did not disturb the activator efficacy of OptoBI-1 but reduced it for Opto-PI and thereby changed the order of efficacies in favor of OptoBI-1 as compared to OptoPI. Upon the photoisomerization of the derivatives, TRPC3 switched rapidly between a basal constitutive activity and a level of current density that is typically observed during maximum G_q-coupled receptor stimulation or direct lipid activation (42).

Fig. 19c displays the peak current to voltage relations obtained for OptoBI-1 and OptoPI (at 365 nm) as well as for OptoBI-2 (at 430 nm) from voltage-ramp recordings. Double rectifying features were evident for the OptoBI-1 and OptoPI-induced conductance, while inward currents were essentially not observed with OptoBI-2. The largest inward currents were observed for OptoBI-1, indicating that profound physiological activity was occurring in terms of the control of TRPC3 Ca^{2+} signaling by this photoswitch (**Fig. 19c**). The maximum inward currents obtained in response to OptoBI-1 were -8,9 ± 2,2 pA/pF (**Fig. 19c-d**) and comparable to that of the parent compound BI-1 (-9,1 ± 2,4 pA/pF, **Fig. 19d**). Specifically, the comparison of the inward current densities revealed that azobenzene modification substantially

impaired the activator efficacy in Opto-PI, significantly reducing the maximum inward current densities from a level of -24,9 ± 5,2 pA/pF, obtained with the parent compound PI (Fig. 1d), to -2,7 ± 1,0 pA/pF determined for Opto-PI (**Fig. 19d**). The inward rectification of these currents was relatively weak as compared to that of the parent compound BI-2 (**Fig. 19b**) and the inward current densities were significantly smaller for OptoBI-2. (OptoBI-2 = - 1,2 ± 0,6 pA/pF vs BI-2 = -21,3 ± 3,5 pA/pF). These results identify OptoBI-1 as an effective TRPC3 photoswitch and a highly promising tool that can be used to exert control over TRPC3 signaling.

Next, we compared the effects of OptoBI-1, OptoBI-2 and OptoPI on Ca^{2+} signaling through recombinant TRPC3 channels by taking Ca^{2+} measurements in HEK293 cells. This heterologous expression system allowed for the use of a genetically encoded Ca^{2+} sensor (R-GECO), which does not interfere with the azobenzene isomerization spectrum.

Ca^{2+} imaging in HEK293 cells co-expressing YFP-TRPC3 and R-GECO was performed along with *cis-trans* isomerization of the GSK photoswitches, triggered by exposure to 10 s illumination periods at 365 nm or 30-s periods at 430 nm. Figure 2e illustrates the time course of the Ca^{2+}-sensitive R-GECO fluorescence in experiments in which the initially extracellular Ca^{2+} was elevated from nominally free to 2 mM in the presence of OptoBI-1 (10 µM) in the dark. Cells exposed to either OptoBI-1 or solvent (DMSO, controls) displayed only small increases in fluorescence upon extracellular Ca^{2+} elevation in the dark (**Fig. 19e**). The results are consistent with the low basal channel activity observed in electrophysiological experiments (Figure 19**c**). UV illumination (365 nm) for a duration of 10 s triggered an elevation in the Ca^{2+}-sensitive fluorescence signal, which was rapidly reverted to baseline levels upon illumination with blue light (430 nm; 30 s). The light-controlled initiation of intracellular Ca^{2+} signals in HEK293 cells was readily repeatable without desensitization when the active state (*cis*-form) of the photoswitch was restricted to relatively short intervals (10 s) as shown for two consecutive cycle activation-deactivation cycles in Figure 19**g**. When cells were exposed for prolonged periods to *cis*-OptoBI-1, as shown for the third activation cycle, slow desensitization/inactivation was evident within a period of

about 1.5 min. Figure 19**h** provides a statistical summary of the changes observed in R-GECO fluorescence by photoisomerization of OptoBI-1. In contrast to OptoBI-1 both OptoBI-2 (not shown) and OptoPI (10 μM, Figure 19**i**) failed to induce significant alterations in cellular Ca^{2+} levels as expected from electrophysiological characterization (Figure 19**c/d**).

7.3.3 Targeting of endogenously expressed ligand-gated TRPC channels in endothelial cells and neurons

Hence, our findings in the HEK293 expression system allowed us to identify OptoBI-1 as an efficient tool that can be used to exert optical control over TRPC3 signaling. This concept was further tested in two cell types that express endogenous TRPC channels and have been previously reported to feature TRPC3 as critical signaling elements in their physiopathology. As TRPC3 is prominently expressed in cardiovascular tissues and the brain [2] we performed experiments in the cell line EA.hy926, which is derived from human umbilical vein endothelium, and in freshly isolated murine hippocampal neurons as test systems. In vascular endothelium TRPC3 has been shown to be essential for Ca^{2+} signaling processes (10,46,47), therefore we investigated whether OptoBI-1 could control TRPC3-mediated Ca^{2+} homeostasis in an endothelial cell background. As shown in **Figure 20a**, native (non-transfected, wild type) EA.hy926 cells were shown to display profound Ca^{2+} transients as measured by fluo-4 fluorescence (at 490 nm), in response to UV (365 nm, 15 s) illumination in the presence of OptoBI-1 (60 μM). This light-induced Ca^{2+} signal was detectable in about 80% of cells (**Figure 20a**). The observation of divergent sensitivity of the endothelial cell population might reflect heterogeneity in terms of TRPC expression levels and/or endothelial phenotype as a determinant of TRPC function (48). The second *cis* OptoBI-1-induced Ca^{2+} transient displayed reduced amplitude, indicating that inactivation /desensitization of the Ca^{2+} entry pathway was taking place. The cells did not respond to the illumination protocol in the absence of the photoswitchable GSK-derivative, and responses were not observed in a nominally Ca^{2+}-free solution, demonstrating that the OptoBI-1-induced response was exclusively due to Ca^{2+} entry (**Figure 20b**). EA.hy926 cells with suppressed TRPC3 expression

due to siRNA knock-down (**Figure 20c**), displayed significantly suppressed responsiveness to *cis*-isomerization of OptoBI-1 **(Figure 20c**). In turn, when TRPC3 channels were overexpressed in the endothelial cells, *cis*-isomerization elicited a significantly larger cellular Ca^{2+} response (**Figure 20a-c**), which were observed in all cells tested (**Figure 20a**), demonstrating the dependence of the light-controlled signaling process on TRPC3 expression.

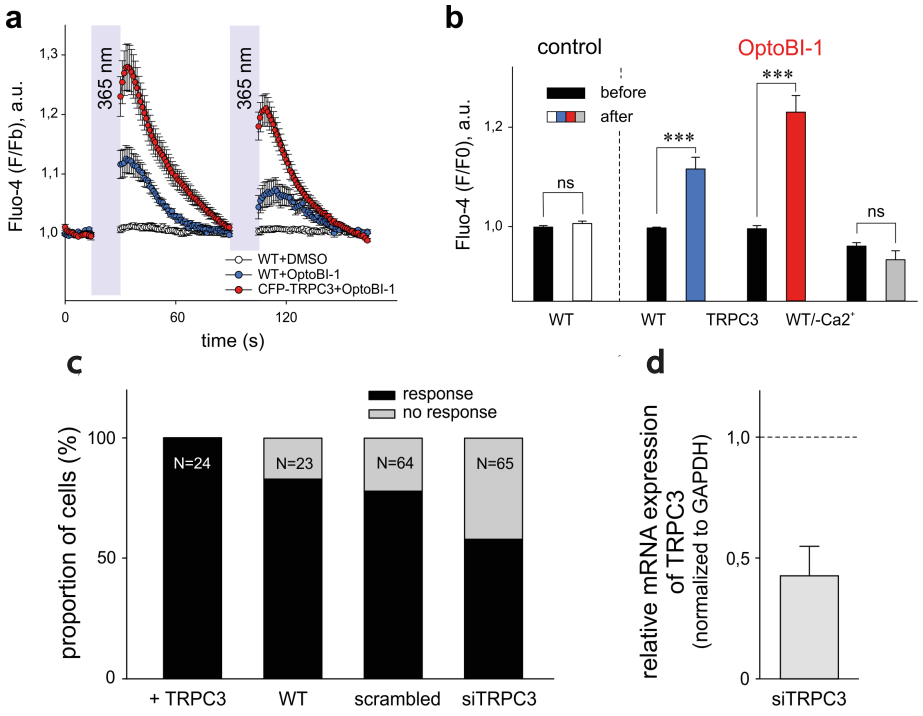

Figure 20. **a,** Time course of Ca^{2+} sensitive Fluo-4 fluorescence in EA.hy926 non-transfected WT cells (control (DMSO) N cells used = 23; OptoBI-1, 60 μM, N = 23) or cells transfected with CFP-TRPC3 (OptoBI-1, 60 μM; N = 21) in 2 mM Ca^{2+} buffer upon *cis*-photoisomerization with UV light (365 nm; 15 s). **b,** Change in bleaching-corrected Fluo-4 fluorescence evoked by *cis*-OptoBI-1 (60 μM) in EA.hy926 cells (WT, N = 23; CFP-TRPC3 transfected, N = 21 and WT in Ca^{2+}-free, N = 10). Control cells (N = 23) were incubated with DMSO in 2 mM Ca^{2+} buffer; statistical significance was tested by two tailed t-test (normally distributed values) or Wilcoxon signed rank test (non-normally distributed values); ns = not significant ($p > 0.05$), ***$p < 0.001$. **c,** Proportion of EA.hy 926 cells responding to UV-induced cis-isomerization of OptoBI-1 (60 μM) with transient increases in Fluo-4 fluorescence in WT cells and after knock-down of TRPC3 with siRNA. OptoBI-1-sensitive (black) and OptoBI-1-insensitive (gray) fraction is shown for non-transfected WT, scrambled- and siTRPC3-transfected EA.hy 926 cells (N = cells is indicated); siRNA-induced reduction is significant ($p<0.05$ and

Chi-square test); **d,** Quantification of TRPC3 knock-down efficiency after treatment with specific siRNA against TRPC3 via real-time PCR using GAPDH as a reference gene. Values of TRPC3 knock-down were normalized to control conditions. Bars represent mean ± SEM (N=3). Figure was done by Niroj Shresta.

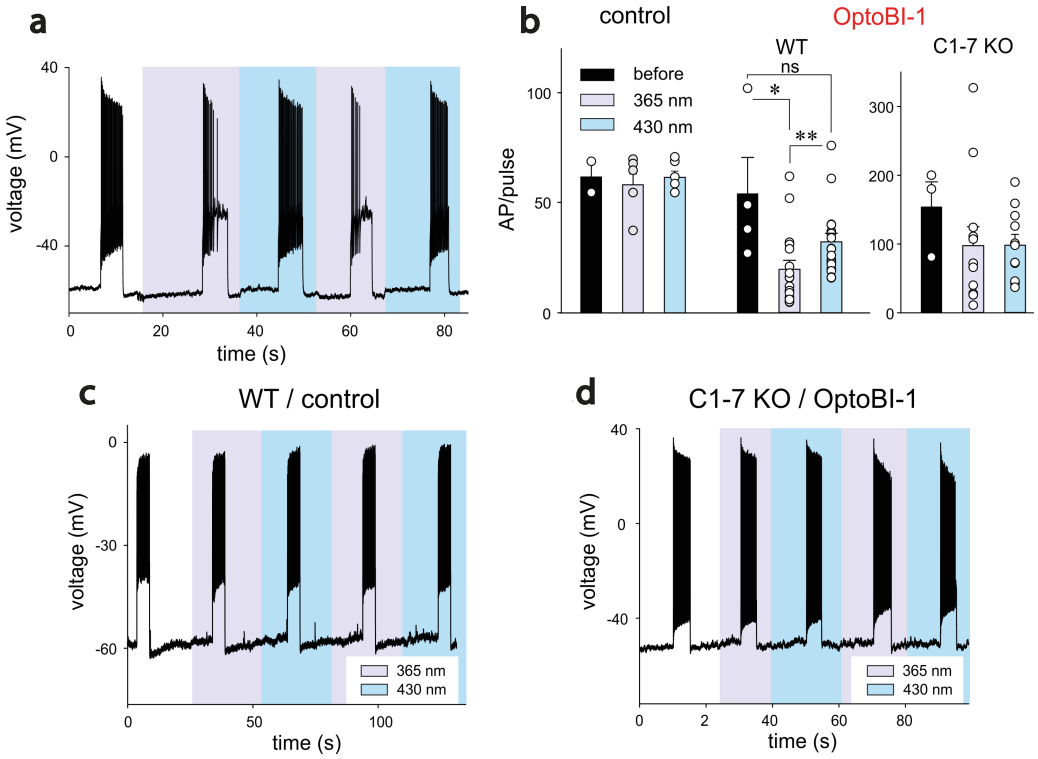

Figure 21. **a,** Representative AP firing in primary hippocampal neurons (WT) induced by a short (5 s) current injection. The first current injection was performed in dark (*trans* conformation; control), following by *cis* isomerization with UV (365 nm) and subsequent reversal to *trans* conformation with blue (430 nm) light. **b,** Mean AP count/pulse in dark, UV and blue light-stimulated in current-clamped WT controls (DMSO) or incubated with OptoBI-1 (20 µM) WT and TRPC1-7 KO neurons. Bar graphs show mean ± SEM from at least 3 different preparations; ns = not significant ($p > 0.05$), *$p < 0.05$; **$p < 0.01$; Statistical significance was tested by two tailed t-test (normally distributed values) or Mann–Whitney tests (non-normally distributed values). Individual values are indicated (circles). **c-d,** Representative AP firing in primary hippocampal neurons WT incubated in DMSO only **(c)** and TRPC1-7 KO incubated with OptoBI-1 (20 µM) **(d).** Firing was induced by short (5 s) current injections in dark (control) and subsequently in UV (365 nm; violet) and in blue (430 nm; blue) light.

In an additional test, we applied OptoBI-1 as a photopharmacological tool to control of neuronal firing. TRPC3 expression and TRPC3 activity levels have been reported to be inversely correlated with the firing of hippocampal neurons in mouse (16). Therefore, we utilized this cell type to test efficiency of our new photoswitch in intact neurons. The electrical activity of cultured murine hippocampal neurons was monitored under whole-cell current clamp conditions, and firing was induced by repetitive depolarizing current injections (5 s, up to 100 pA) in the presence of OptoBI-1 (20 μM). The cyclic, light-induced photoisomerization of the activator was initiated after a control period to stabilize neuronal activity. UV light-induced *cis*-isomerization, (30 s) significantly reduced firing during the current injections (**Figure 21a-b**). This light-induced suppression of neuronal activity was virtually instantaneous and could be rapidly reverted by *trans*-isomerization of OptoBI-1 (430 nm), albeit to a level slightly lower than that of the control. Subsequently, it was possible perform the light-controlled cycling of neuronal firing between constant minimum and maximum levels for more than 5 times without observing apparent desensitization. The results of control experiments run in the absence of OptoBI-1 demonstrated that the alteration in neuronal activity was mediated by OptoBI-1 (**Figure 21c**). The observed inhibition by *cis*-OptoBI-1, which activates TRPC channels is consistent with the reported inverse correlation of TRPC3 activity and hippocampal firing (16). The mechanism of this connection is still elusive, but may involve local Ca^{2+} signaling. The fact that a complete reversal of firing suppression was not achieved upon illumination with blue light (430 nm) may be explained by a high affinity interaction of the *cis*-isomer. This does not seem to be entirely eliminated by the photoconversion protocol. The dependency of OptoBI-1 effects on TRPC expression in this cell model was shown by the use of hippocampal neurons isolated from a mouse model that lacks all seven canonical TRPC isoforms ($TRPC_{1-7}$ KO) (30,49). Photoisomerization failed to induce a significant cycling of firing frequency in $TRPC_{1-7}$ KO neurons, substantiating the conclusion that optical control was indeed achieved by interference with hippocampal TRPC activity. A trend towards lower activity levels during photoisomerization was again observed, however this phenomenon was not statistically significant (**Figure 21d**).

8. Discussion

8.1 Off-target effects of the coumarin moiety released during photouncaging

Despite the general value of caged ligands including caged lipids and the increasing interest to their potential, specificity of this photopharmacological approach is poorly characterized. Photopharmacological caging by linkage of the active structure to a coumarin moiety has been used for a wide range of second messengers (50). An interesting application of coumarin uncaging was reported by Furuta et al. who used caged cyclic guanosine monophosphate to control ion channels (CNGCs) in olfactory sensory cells (51). Cell were loaded with the caged cyclic nucleotide via a patch pipette, which presumably enabled to minimize the non-specific effects of the caged ligand and the uncaging byproducts on off target proteins and the plasma membrane. As it was previously shown by Nadler et al., that caged diacylglycerols exert a rather specific action in terms of optical control of TRPC channels but were characterized exclusively by monitoring intracellular Ca^{2+} transients with fluorescence probes. We aimed to further characterize the specificity of uncaged DAGs to manipulate TRPC3 conductances. However, electrophysiological experiments revealed failure of Bhcmoc-1,2-DOG to selectively manipulate TRPC3 currents in transfected HEK293 cells upon photouncaging. We observed non-selective, UV-induced currents distinctly different from those based on a response of TRPC3 to the lipid mediator in transfected HEK293 cells. As Ca^{2+} ions inhibit TRPC3 activity (52), we performed experiments in nominally Ca^{2+}-free conditions to augment the current component based on TRPC3 activation. We could trace functional TRPC3 channels activity but these currents were still largely buried behind a dominating, ill-defined non-specific conductance. Eventually, by combination of Ca^{2+} free conditions and SKF 96365 as a TRPC blocker, we succeeded to reduce the non-specific conductance in TRPC3-transfected cells to the level observed in control, wild-type HEK cells. Further, detailed investigation of the TRPC3-independent conductance led us to hypothesis that coumarin as a photoreleased moiety might itself interact with the

plasma membrane to produce an off-target effect. Coumarin by itself does not absorb UV light; however, certain derivatives are sensitive to UV irradiation (33). The natural coumarin derivative psoralen had been successfully employed for clinical treatment in dermatology (53). Psoralen photoreacts with UV and promotes production of reactive oxygen species such as superoxide and singlet oxygen which result in cell damage (54). Thus, we tested coumarin and coumarin derivatives (**Figure 4**) on wild-type HEK cells and TRPC3 overexpressing HEK293 cells. Non-modified coumarin (**1d, Figure 4**) was not producing any conductance in the presence of UV illumination (340 nm), which was used to uncage lipid from Bhcmoc-1,2-DOG. On the contrary, coumarin derivatives **1a-c**, that are commonly used as caging molecules in photopharmacological experiments, induced a similar current as observed after photostimulation of Bhcmoc-1,2-DOG (29).

Interestingly, the currents induced by photoactivation of coumarin derivatives, were not well correlated with intracellular Ca^{2+} measurements, where 10 s pulses of UV light were inefficient to initiate any cytosolic Ca^{2+} signals in the but elicited non-specific currents in wild-type HEK293 cells. We assumed that the observed phototriggered membrane conductance in the presence of coumarin derivatives was not carried by calcium cations. A subsequent series of experiments involving the well-established classical blocker of cation channels Ruthenium Red (data not shown) and SKF 96365 failed to effect the coumarin-induced conductance. As a next step, we performed ion selectivity experiments where each of the ions of the bath solution one by one was replaced or removed from the buffer. The reversal potential of TRPC3 channels in normal physiological ion gradients and activated by DAGs is between +4 and +11 mV. Therefore, we monitored the change in reversal potential in altered buffer composition: when Cl^- in the bath solution was reduced from 148 to 2 mM (replaced by gluconate), the reversal potential did not change significantly; replacement of Na^+ by NMDG caused shift in reversal potential from +5.1±1.9 to -9.3±2.4 mV (data not shown) but still it was not significant. Nevertheless, considering the ability of coumarins to produce reactive oxygen species, we cannot completely exclude that the conductance, observed upon photoactivation, is rather a nonspecific,

phototoxic effect on the membrane lipid organization that generates a leak through the plasma membrane (29).

Despite the clear advantages of caged ligands approachs, coumarin-caged ligands bear the risk of hidden side-effects. Our findings suggest that results from photopharmacological application of coumarin-caged messengers have to be considered with particular care for the action of photoactivated coumarin cages on plasma membrane integrity (29).

8.2 A photochromic ligand approach enables a close look into the gating and lipid sensing process in TRPC3 channels

To utilize the photopharmacological venue for a gain in depth insight into TRPC protein function, we employed a photochromic ligand approach. Combination of homology modeling and our newly synthetized photoswitchable DAG (OptoDArG) was successfully used the high temporal and quantitative precision of optical control to uncover the structural basis of lipid-protein interactions (“Reproduced from (14) with permission of publisher Nature Chemical Biology, Springer Nature Limited, 2018”).

In an attempt to identify the molecular elements responsible for lipid discrimination by TRPC3 channels, we compared two light-sensing lipid species, OptoDArG and previously introduce PhoDAG-1 (34). We found that OptoDArG induced larger conductances through TRPC3 and G652A channels demonstrating the ability to discriminate well between lipid species. Interestingly the amplitude of G652A response was much larger. Quantitative analysis of the TRPC3 wild-type and mutant conductances induced by OptoDArG revealed a significant reduction in threshold of G652A activation. Change in efficiency and potency of OptoDArG in mutant suggested a possible alteration in cooperativity between the subunits. We introduced an optical “lipid-clamp” to precisely monitor on and off kinetics of the channel activity. Superfast photoswitching of OptoDArG allowed to clearly discern an altered delay of activation in mutant channels indicating an increased sensitivity to the particular photolipid. We also noticed that the activation kinetics was clearly sigmoidal.

Sigmoidicity implies the involvement of multiple conformational changes within a protein complex, which are required to obtain full channel opening. This means that each subunit of the channel may undergo identical and independent conformational transitions prior to the final opening (55). For homotetrameric channels, like TRPC3, the four-fold symmetry implies 4 lipid interaction sites and 4 independent conformational transitions resulting in a power (*n*) of at least 4 for the whole complex. Therefore, the observed reduction of *n* in G652A (from 5 in WT to 3 in mutant) for photostimulation by OptoDArG was an indication of a significant change in cooperativity within the channel. We also considered the possibility of a faster interaction and on-kinetics of mutant-lipid interactions for OptoDArG as the basis of shortened activation. Additionally, we suspected that the presence of native lipids of the plasma membrane together with enhanced affinity of individual lipid recognition sites in the mutated channels might cause the hastened channel activation ("Reproduced from (14) with permission of publisher Nature Chemical Biology, Springer Nature Limited, 2018").

Interesting to note, this residue is well conserved through the whole TRPC subfamily and may serve as a general lipid sensing site for all TRPCs especially considering the recent finding of DAG sensing by TRPC4 and TRPC5 channels (7) ("Reproduced from (14) with permission of publisher Nature Chemical Biology, Springer Nature Limited, 2018").

Collectively, the described features of G652A mutant point towards a crucial and essential functional role of this element, which is localized within the pore TRPC3 architecture and at subunit-joining fenestrations. This structure enables association with lipids and determines further channel opening. However, whether the glycine in the position 652 functions as primary lipid sensor or an indirect allosteric determinant of the primary lipid sensor is still unclear and needs to be clarified (14). In support of our conclusion, glycine residue in position 652 (G640 in isoform 1) was later found in a lipid occupied region by Fan et al. who recently resolved the TRPC3 structure by single particle cryo electron microscopy (12) ("Reproduced from (14) with permission of publisher Nature Chemical Biology, Springer Nature Limited, 2018").

8.3 Selective photoswitchable ligand manipulates endogenously expressed TRPC channels in endothelial cells and neurons

Considering inability of OptoDArG to discriminate between lipid-dependent proteins in native tissue and to target specifically TRPC channels, we developed an alternative way to to control endogenous TRPCs. In aggregate, our results obtained in experiments with vascular endothelial and neuronal cells confirm the value of OptoBI-1 as an effective photoswitch for a precise light-dependent control of TRPC activity. OptoBI-1 allowed us temporally manipulate of Ca^{2+} transients via TRPC-mediated signaling processes in human vascular endothelial cells and reduction of firing in murine hippocampal neurons. This novel tool is expected to help researches gain a better understanding of TRPC physiopathology for a development of new therapeutic strategies to target these ion channels in native tissues.

Bibliography:

1. Riccio A, Medhurst AD, Mattei C, Kelsell RE, Calver AR, Randall AD, et al. mRNA distribution analysis of human TRPC family in CNS and peripheral tissues. Brain Res Mol Brain Res. 2002 Dec 30;109(1-2):95–104.

2. Clapham DE. TRP channels as cellular sensors. Nature. Nature Publishing Group; 2003 Dec 4;426(6966):517–24.

3. Kunert-Keil C, Bisping F, Krüger J, Brinkmeier H. BMC Genomics. BMC Genomics. 2006;7(1):159–14.

4. Tiapko O, Groschner K. TRPC3 as a Target of Novel Therapeutic Interventions. Cells. Multidisciplinary Digital Publishing Institute; 2018 Jul 22;7(7):83.

5. Vazquez G, Wedel BJ, Aziz O, Trebak M, Putney JW Jr. The mammalian TRPC cation channels. Biochimica et Biophysica Acta (BBA) - Molecular Cell Research. 2004 Dec;1742(1-3):21–36.

6. Wang Y, Bu J, Shen H, Li H, Wang Z, Chen G. Targeting Transient Receptor Potential Canonical Channels for Diseases of the Nervous System. CDT. 2017 Aug 24;18(12):1–165.

7. Storch U, Forst A-L, Pardatscher F, Erdogmus S, Philipp M, Gregoritza M, et al. Dynamic NHERF interaction with TRPC4/5 proteins is required for channel gating by diacylglycerol. Proc Natl Acad Sci USA. 2017 Jan 3;114(1):E37–E46.

8. Hofmann T, Obukhov AG, Schaefer M, Harteneck C, Gudermann T, Schultz G. Direct activation of human TRPC6 and TRPC3 channels by diacylglycerol. Nature. Nature Publishing Group; 1999 Jan 21;397(6716):259–63.

9. Strübing C, Krapivinsky G, Krapivinsky L, Clapham DE. Formation of Novel TRPC Channels by Complex Subunit Interactions in Embryonic Brain. J Biol Chem. 2003 Sep 26;278(40):39014–9.

10. Kamouchi M, Philipp S, Flockerzi V, Wissenbach U, Mamin A, Raeymaekers L, et al. Properties of heterologously expressed hTRP3 channels in bovine pulmonary artery endothelial cells. Journal of Physiology. 1999 Jun 23;2(518):345–58.

11. Vazquez G, Lievremont JP, St J Bird G, Putney JW. Human Trp3 forms both inositol trisphosphate receptor-dependent and receptor-independent store-operated cation channels in DT40 avian B lymphocytes. Proceedings of the National Academy of Sciences. National Academy of

Sciences; 2001 Sep 11;98(20):11777–82.

12. Fan C, Choi W, Sun W, Du J, Lu W. Structure of the human lipid-gated cation channel TRPC3. eLife. eLife Sciences Publications Limited; 2018 May 4;7:e36852–14.

13. Tang Q, Guo W, Zheng L, Wu J-X, Liu M, Zhou X, et al. Structure of the receptor-activated human TRPC6 and TRPC3 ion channels. Cell Research. Springer US; 2018 Apr 19;:1–10.

14. Lichtenegger M, Tiapko O, Svobodova B, Stockner T, Glasnov TN, Schreibmayer W, et al. An optically controlled probe identifies lipid-gating fenestrations within the TRPC3 channel. Nature Chemical Biology. Springer US; 2018 Feb 23;14(4):1–9.

15. Hartmann J, Dragicevic E, Adelsberger H, Henning HA, Sumser M, Abramowitz J, et al. TRPC3 Channels Are Required for Synaptic Transmission and Motor Coordination. Neuron. 2008 Aug;59(3):392–8.

16. Neuner SM, Wilmott LA, Hope KA, Hoffmann B, Chong JA, Abramowitz J, et al. TRPC3 channels critically regulate hippocampal excitability and contextual fear memory. Behavioural Brain Research. 2015 Mar;281:69–77.

17. Becker EBE, Oliver PL, Glitsch MD, Banks GT, Achilli F, Hardy A, et al. A point mutation in TRPC3 causes abnormal Purkinje cell development and cerebellar ataxia in moonwalker mice. Proceedings of the National Academy of Sciences. National Academy of Sciences; 2009 Apr 21;106(16):6706–11.

18. Fogel BL, Hanson SM, Becker EBE. Do mutations in the murine ataxia gene TRPC3 cause cerebellar ataxia in humans? Obeso MD PhD JA, Stacy Chair M-SEBM, Lang A, Napier C, Samuel M, Strafella A, et al., editors. Mov Disord. Wiley-Blackwell; 2015 Feb;30(2):284–6.

19. Min S-J, Kang T-C. Positive feedback role of TRPC3 in TNF-α-mediated vasogenic edema formation induced by status epilepticus independent of ETB receptor activation. Neuroscience. 2016 Nov 19;337:37–47.

20. Huang J-H, He G-W, Xue H-M, Yao X-Q, Liu X-C, Underwood MJ, et al. TRPC3 channel contributes to nitric oxide release: significance during normoxia and hypoxia–reoxygenation. Cardiovascular Research. 2011 Apr 14;91(3):472–82.

21. Lemonnier L, Trebak M, Putney JW Jr. Complex regulation of the TRPC3, 6 and 7 channel subfamily by diacylglycerol and phosphatidylinositol-4,5-bisphosphate. Cell Calcium. 2008 May;43(5):506–14.

22. Xu X, Lozinskaya I, Costell M, Lin Z, Ball JA, Bernard R, et al. Characterization of Small Molecule TRPC3 and TRPC6 agonist and Antagonists. Biophysj. Biophysical Society; 2013 Jan 29;104(S1):454a.

23. Qu C, Ding M, Zhu Y, Lu Y, Du J, Miller M, et al. Pyrazolopyrimidines as Potent Stimulators for Transient Receptor Potential Canonical 3/6/7 Channels. J Med Chem. 2017 Apr 28;60(11):4680–92.

24. Doleschal B, Primessnig U, Wolkart G, Wolf S, Schernthaner M, Lichtenegger M, et al. TRPC3 contributes to regulation of cardiac contractility and arrhythmogenesis by dynamic interaction with NCX1. Cardiovascular Research. 2015 Mar 17;106(1):163–73.

25. Numaga-Tomita T, Kitajima N, Kuroda T, Nishimura A, Miyano K, Yasuda S, et al. TRPC3-GEF-H1 axis mediates pressure overload-induced cardiac fibrosis. Scientific Reports. Nature Publishing Group; 2016 Dec 6;:1–12.

26. Poteser M, Graziani A, Eder P, Yates A, Mächler H, Romanin C, et al. Identification of a rare subset of adipose tissue-resident progenitor cells, which express CD133 and TRPC3 as a VEGF-regulated Ca 2+entry channel. FEBS Letters. 2008 Jul 9;582(18):2696–702.

27. Koenig S, Schernthaner M, Maechler H, Kappe CO, Glasnov TN, Hoefler G, et al. A TRPC3 blocker, ethyl-1-(4-(2,3,3-trichloroacrylamide)phenyl)-5-(trifluoromethyl)-1H-pyrazole-4-carboxylate (Pyr3), prevents stent-induced arterial remodeling. J Pharmacol Exp Ther. 2013 Jan;344(1):33–40.

28. Nadler A, Reither G, Feng S, Stein F, Reither S, Müller R, et al. The fatty acid composition of diacylglycerols determines local signaling patterns. Angew Chem Int Ed Engl. Wiley-Blackwell; 2013 Jun 10;52(24):6330–4.

29. Tiapko O, Bacsa B, la Cruz de GG, Glasnov T, Groschner K. Optopharmacological control of TRPC channels by coumarin-caged lipids is associated with a phototoxic membrane effect. Sci China Life Sci. 2016 Jul 19;59(8):802–10.

30. Lutas A, Birnbaumer L, Yellen G. Metabolism Regulates the Spontaneous Firing of Substantia Nigra Pars Reticulata Neurons via K ATPand Nonselective Cation Channels. Journal of Neuroscience. 2014 Dec 3;34(49):16336–47.

31. Singh A, Hildebrand ME, Garcia E, Snutch TP. The transient receptor potential channel antagonist SKF96365 is a potent blocker of low-voltage-activated T-type calcium channels. Br J Pharmacol. Wiley/Blackwell (10.1111); 2010 Jul;160(6):1464–75.

32. Zhu MX, Tang J. TRPC channel interactions with calmodulin and IP3

receptors. Novartis Found Symp. 2004;258:44–58–discussion58–62–98–102–263–6.

33. Zou Q, Fang Y, Zhao Y, Zhao H, Wang Y, Gu Y, et al. Synthesis and in vitro photocytotoxicity of coumarin derivatives for one- and two-photon excited photodynamic therapy. J Med Chem. American Chemical Society; 2013 Jul 11;56(13):5288–94.

34. Frank JA, Yushchenko DA, Hodson DJ, Lipstein N, Nagpal J, Rutter GA, et al. Photoswitchable diacylglycerols enable optical control of protein kinase C. Nature Chemical Biology. Nature Publishing Group; 2016 Jul 25;12(9):755–62.

35. Cao E, Liao M, Cheng Y, Julius D. TRPV1 structures in distinct conformations reveal activation mechanisms. Nature. Nature Publishing Group; 2013 Dec 5;504(7478):113–8.

36. Liu X, Singh BB, Ambudkar IS. TRPC1 is required for functional store-operated Ca2+ channels. Role of acidic amino acid residues in the S5-S6 region. J Biol Chem. American Society for Biochemistry and Molecular Biology; 2003 Mar 28;278(13):11337–43.

37. Poteser M, Schleifer H, Lichtenegger M, Schernthaner M, Stockner T, Kappe CO, et al. PKC-dependent coupling of calcium permeation through transient receptor potential canonical 3 (TRPC3) to calcineurin signaling in HL-1 myocytes. Proc Natl Acad Sci USA. National Academy of Sciences; 2011 Jun 28;108(26):10556–61.

38. Lichtenegger M, Stockner T, Poteser M, Schleifer H, Platzer D, Romanin C, et al. A novel homology model of TRPC3 reveals allosteric coupling between gate and selectivity filter. Cell Calcium. Elsevier Ltd; 2013 Sep 1;54(3):175–85.

39. Frank JA, Moroni M, Moshourab R, Sumser M, Lewin GR, Trauner D. Photoswitchable fatty acids enable optical control of TRPV1. Nature Communications. Nature Publishing Group; 2015 May 22;6(1):7118–11.

40. Zagotta WN, Hoshi T, Dittman J, Aldrich RW. Shaker potassium channel gating. II: Transitions in the activation pathway. J Gen Physiol. The Rockefeller University Press; 1994 Feb;103(2):279–319.

41. Leinders-Zufall T, Storch U, Bleymehl K, Schnitzler MMY, Frank JA, Konrad DB, et al. PhoDAGs Enable Optical Control of Diacylglycerol-Sensitive Transient Receptor Potential Channels. Cell Chemical Biology. Elsevier Ltd; 2017 Dec 5;:1–13.

42. Lichtenegger M, Tiapko O, Svobodova B, Stockner T, Glasnov TN,

Schreibmayer W, et al. An optically controlled probe identifies lipid- gating fenestrations within the TRPC3 channel. Nature Chemical Biology. Springer US; 2018 Mar 1;:1–17.

43. Kiyonaka S, Kato K, Nishida M, Mio K, Numaga T, Sawaguchi Y, et al. Selective and direct inhibition of TRPC3 channels underlies biological activities of a pyrazole compound. Proceedings of the National Academy of Sciences. National Academy of Sciences; 2009 Mar 31;106(13):5400–5.

44. Washburn DG, Holt DA, Dodson J, McAtee JJ, Terrell LR, Barton L, et al. The discovery of potent blockers of the canonical transient receptor channels, TRPC3 and TRPC6, based on an anilino-thiazole pharmacophore. Bioorganic & Medicinal Chemistry Letters. Elsevier Ltd; 2013 Sep 1;23(17):4979–84.

45. Guedes de la Cruz G, Svobodova B, Lichtenegger M, Tiapko O, Groschner K, Glasnov T. Intensified Microwave-Assisted N-Acylation Procedure – Synthesis and Activity Evaluation of TRPC3 Channel Agonists with a 1,3-Dihydro-2H-benzo[d]imidazol-2-one Core. Synlett. 2017 Mar 16;28(06):695–700.

46. Groschner K, Hingel S, Lintschinger B, Balzer M, Romanin C, Zhu X, et al. Trp proteins form store-operated cation channels in human vascular endothelial cells. FEBS Letters. 1998 Oct 16;437(1-2):101–6.

47. Poteser M, Graziani A, Rosker C, Eder P, Derler I, Kahr H, et al. TRPC3 and TRPC4 associate to form a redox-sensitive cation channel. Evidence for expression of native TRPC3-TRPC4 heteromeric channels in endothelial cells. J Biol Chem. American Society for Biochemistry and Molecular Biology; 2006 May 12;281(19):13588–95.

48. Graziani A, Poteser M, Heupel W-M, Schleifer H, Krenn M, Drenckhahn D, et al. Cell-cell contact formation governs Ca2+ signaling by TRPC4 in the vascular endothelium: evidence for a regulatory TRPC4-beta-catenin interaction. J Biol Chem. American Society for Biochemistry and Molecular Biology; 2010 Feb 5;285(6):4213–23.

49. Birnbaumer L. From GTP and G proteins to TRPC channels: a personal account. J Mol Med. Springer Berlin Heidelberg; 2015 Sep 16;93(9):941–53.

50. Mayer G, Heckel A. Biologically active molecules with a "light switch". Vol. 45, Angewandte Chemie (International ed. in English). 2006. pp. 4900–21.

51. Furuta T, Takeuchi H, Isozaki M, Takahashi Y, Kanehara M, Sugimoto M, et al. Bhc-cNMPs as either water-soluble or membrane-permeant

photoreleasable cyclic nucleotides for both one- and two-photon excitation. Chembiochem. 2004 Aug 6;5(8):1119–28.

52. Rosker C, Graziani A, Lukas M, Eder P, Zhu MX, Romanin C, et al. Ca(2+) signaling by TRPC3 involves Na(+) entry and local coupling to the Na(+)/Ca(2+) exchanger. J Biol Chem. 2004 Apr 2;279(14):13696–704.

53. Mantulin WW, Song PS. Excited states of skin-sensitizing coumarins and psoralens. Spectroscopic studies. J Am Chem Soc. 1973 Aug 8;95(16):5122–9.

54. Park SC, Goodrich RP, Yerram N, Sowemino-Coker SO, Platz MS, Aquila B. Photodynamic inactivation of viral and bacterial blood contaminants with halogenated coumarin and furocoumarin sensitizers.

WO1996008965A1, 1996. pp. 1–113.

55. HODGKIN AL, HUXLEY AF. A quantitative description of membrane current and its application to conduction and excitation in nerve. The Journal of Physiology. Wiley-Blackwell; 1952 Aug;117(4):500–44.